Horizontal Variability of 2-m Temperature at Night during CASES-97

MARGARET A. LEMONE AND KYOKO IKEDA

National Center for Atmospheric Research, Boulder, Colorado*

ROBERT L. GROSSMAN

Colorado Research Associates, Boulder, Colorado

MATHIAS W. ROTACH

Swiss Federal Institute of Technology, Zurich, Switzerland

(Manuscript received 13 May 2002, in final form 29 January 2003)

ABSTRACT

Surface-station, radiosonde, and Doppler minisodar data from the Cooperative Atmosphere–Surface Exchange Study-1997 (CASES-97) field project, collected in a 60-km-wide array in the lower Walnut River watershed (terrain variation ~150 m) southeast of Wichita, Kansas, are used to study the relationship of the change of the 2-m potential temperature Θ_{2m} with station elevation z_e, $\partial\Theta_{2m}/\partial z_e \equiv \Theta_{,ze}$ to the ambient wind and thermal stratification $\partial\Theta/\partial z \equiv \Theta_{,z}$ during fair-weather nights. As in many previous studies, predawn Θ_{2m} varies linearly with z_e, and $\Theta_{,ze} \sim \Theta_{,z}$ over a depth h that represents the maximum elevation range of the stations. Departures from the linear Θ_{2m}–elevation relationship ($\Theta_{,ze}$ line) are related to vegetation (cool for vegetation, warm for bare ground), local terrain (drainage flows from nearby hills, although a causal relationship is not established), and the formation of a cold pool at lower elevations on some days.

The near-surface flow and its evolution are functions of the Froude number Fr = $S/(Nh)$, where S is the mean wind speed from the surface to h, and N is the corresponding Brunt–Väisälä frequency. The near-surface wind is coupled to the ambient flow for Fr = 3.3, based on where the straight line relating $\Theta_{,ze}$ to ln Fr intersects the ln Fr axis. Under these conditions, Θ_{2m} is constant horizontally even though $\Theta_{,z} > 0$, suggesting that near-surface air moves up- and downslope dry adiabatically. However, Θ_{2m} cools (or warms) everywhere at the same rate. The lowest Froude numbers are associated with drainage flows, while intermediate values characterize regimes with intermediate behavior. The evolution of Θ_{2m} horizontal variability σ_Θ through the night is also a function of the predawn Froude number. For the nights with the lowest Fr, the σ_Θ maximum occurs in the last 1–3 h before sunrise. For nights with Fr ~ 3.3 ($\Theta_{,ze} \approx 0$) and for intermediate values, σ_Θ peaks 2–3 h after sunset. The standard deviations relative to the $\Theta_{,ze}$ line reach their lowest values in the last hours of darkness. Thus, it is not surprising that the relationships of $\Theta_{,ze}$ to Fr and $\Theta_{,z}$ based on data through the night show more scatter, and $\Theta_{,ze} \sim 0.5\Theta_{,z}$ in contrast to the predawn relationship. However, $\Theta_{,ze} \approx 0$ for ln Fr = 3.7, a value similar to that just before sunrise.

A heuristic Lagrangian parcel model is used to explain the horizontal uniformity of time-evolving Θ_{2m} when the surface flow is coupled with the ambient wind, as well as both the linear variation of Θ_{2m} with elevation and the time required to reach maximum values of σ_Θ under drainage-flow conditions.

1. Introduction

The objective of this paper is to examine the role of planetary boundary layer processes, terrain, and surface cover in the nighttime horizontal distribution of Θ_{2m}, the 0.5-h-averaged potential temperature 2 m above the surface, under undisturbed conditions. We use surface Mesonet, Doppler minisodar, 915-MHz radar wind profiler, and radiosonde data from the lower Walnut River watershed southeast of Wichita, Kansas, collected during the Cooperative Atmosphere–Surface Exchange Study-1997 (CASES-97) field project (LeMone et al. 2000). The lower watershed, where observations were concentrated, is ~50 km across, and the terrain elevation range is ~150 m (Fig. 1). The watershed-scale patterns discussed in this paper provide at least a partial context for the observations of turbulence-generating

* The National Center for Atmospheric Research is partially supported by the National Science Foundation.

Corresponding author address: Margaret A. LeMone, NCAR, P.O. Box 3000, Boulder, CO 80307-3000.
E-mail: lemone@ucar.edu

© 2003 American Meteorological Society

Unauthenticated | Downloaded 08/01/21 08:40 PM UTC

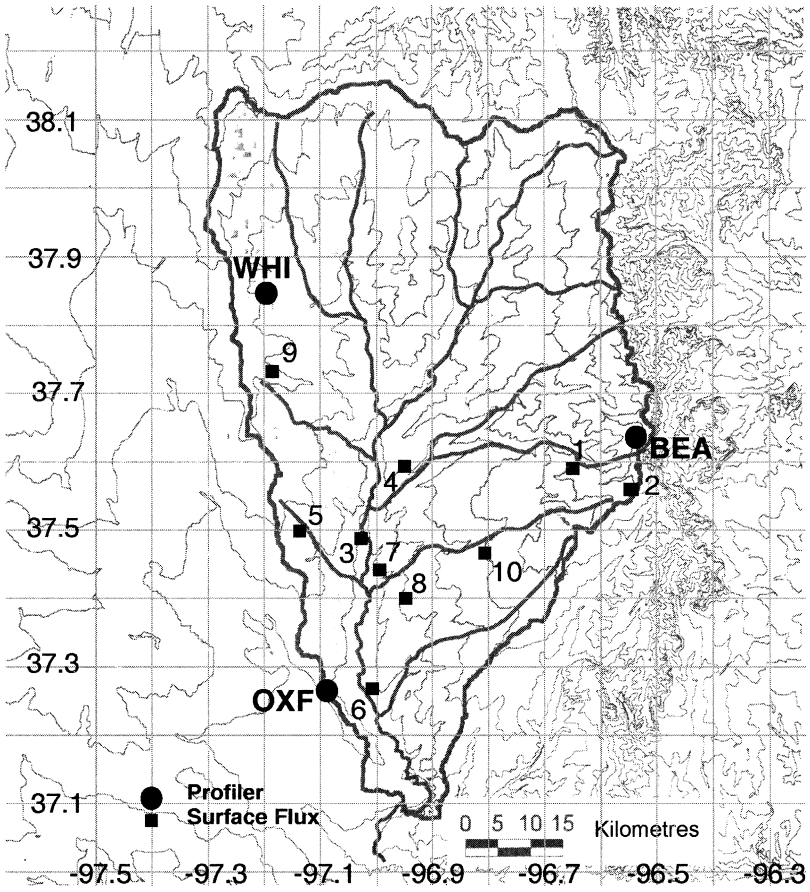

FIG. 1. CASES-97 array superposed on a contour map of the Walnut River watershed. Numbers denote surface flux stations, sited according to elevation and surface cover; data from stations 1–8 are used here. Beaumont (BEA), Oxford (OXF), and Whitewater (WHI) are sites of wind-profiling systems operated by the Argonne National Laboratory; radiosondes were released from these sites at 90-min intervals during IOPs. Contour interval is 20 m; the north–south river is the Walnut.

phenomena in CASES-99 (Poulos et al. 2002), which took place in the same watershed 2.5 yr later but with most measurements concentrated over a smaller area.

While near-surface air temperatures are relatively uniform horizontally during the day, horizontal variability increases during the night, and much of that variability is related to station elevation. Figure 2 illustrates the horizontal variability of temperature over the CASES array for 46 h centered at 1200 CST 10 May 1997. LeMone et al. (2002) summarize the behavior of the daytime temperature pattern, showing that it responds mainly to the vertical divergence of the vertical heat flux, and secondarily to horizontal advection and the effects of local surface cover. However, the nearly uniform daytime pattern changes drastically around sunset and continues to evolve through the night. By early morning, the temperature is mainly a function of station elevation z_e, with the temperature difference between the highest and lowest stations (thick lines) maximum just before sunrise on 10 May, when the temperatures reach their nocturnal minimum. This dependence is close to linear, as illustrated by Fig. 3. The presunrise 2-m temperature change with elevation z_e, $\partial T_{2m}/\partial z_e$, for the 2 days are 0.076 K m^{-1} and 0.020 K m^{-1}, respectively. Note that the standard deviations for the two lines are similar, even though the correlation coefficient R is less for 11 May.

The association of cooler early morning minimum temperatures with lower elevations must have been noticed as long as farmers struggled with killing frosts, but the linear dependence of minimum surface air temperature on elevation in rolling to hilly terrain has been documented only during the last several decades (Table 1). Harrison (1971) noted that the linear relationship worked best when temperatures were relative to the temperatures at the local valley floor. Acevedo and Fitzjarrald (2001, hereafter referred to as AF) found a good linear relationship between each station's height relative to the surrounding 3 km $\times$ 3 km area and its temperature relative to the domain average, but only a fair relationship between absolute station elevation and its temperature relative to the domain average. Rather than using

Unauthenticated | Downloaded 08/01/21 08:40 PM UTC

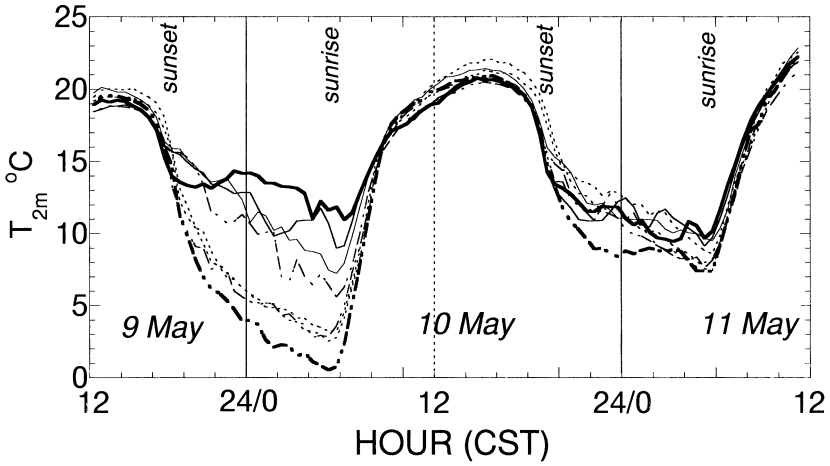

FIG. 2. For stations 1–8 in Fig. 1, horizontal variation of diurnal variability in 30-min-averaged 2-m temperature for a 2-day period. Type of line denotes surface cover. Solid line represents grass; dotted–dashed line, winter wheat; and dotted line, bare ground with seedlings or weeds by mid-May. Heavy solid line is temperature at the highest elevation site (station 2, grassland); heavy dashed–dotted line is temperature at the lowest elevation site (station 6, winter wheat).

minimum temperature, they used temperatures at the time of maximum horizontal variability (1–3 h after sunset[1]) for their data.

As illustrated in Fig. 2, the linear relationship between Θ_{2m} and elevation emerges during the night. The horizontal variability of Θ_{2m} at night evolves in response to radiative cooling and ambient wind. Nocturnal radiative cooling under clear skies and weak winds creates drainage flows, relatively cool air flowing downhill by virtue of its negative buoyancy. As noted in the classical studies of such flows (e.g., Fleagle 1950), the fact that air cools more rapidly near the surface than higher up leads to negatively buoyant shallow currents flowing down slopes into valleys, where the cold air ''pools.'' The downslope flows are reinforced by stronger radiative cooling in exposed areas, such as ridges (e.g., Geiger 1966). The surface flow characteristics change with stronger winds or weaker radiative cooling (e.g., Gudicksen et al. 1992; AF; van de Wiel et al. 2002). When the ambient winds are sufficiently strong or nocturnal cooling sufficiently weak, vertical turbulent mixing couples the surface layer to the ambient flow. For intermediate conditions, such coupling becomes more intermittent, but local drainage flows can still develop (Mahrt et al. 2001). No explanation has been offered for why such processes lead to a linear variation of T_{2m} with elevation.

Research on flow over hills and in valleys suggests that a form of the Froude number Fr defines the conditions separating drainage flow from flow coupled to the ambient wind. Several authors have discussed flow over hills in stable stratification (e.g., Jackson and Hunt 1975; Carruthers and Hunt 1990; Belcher and Hunt 1998), relating two-dimensional flow regimes to two forms of the Froude number $S/(Nh)$ or $S/(NL)$ where S is the wind speed, $N \equiv [(g/\Theta_v)(\partial\Theta_v/\partial z)]^{1/2}$ is the Brunt–Väisälä frequency, g is the acceleration of gravity, Θ_v is the virtual potential temperature, h is the height of the hill, and L is the horizontal wavelength of the hill. Smith (1989) discusses such idealized flow around an isolated hill in three dimensions. Mason (1987) is the first to apply Froude-number scaling to flow in valleys, showing that observed ambient flow remains ''coupled'' to the valley for $\mathrm{Fr} = S/(Nh) > 2$, for cases with the wind direction within 30° of normal to the valley. These results were confirmed in a later study by Holden et al. (2000), replacing S by the speed of the wind normal to the terrain. The terrain slopes for the two valleys—0.2–0.3 for Mason and ~0.3 for Holden et al.—are much

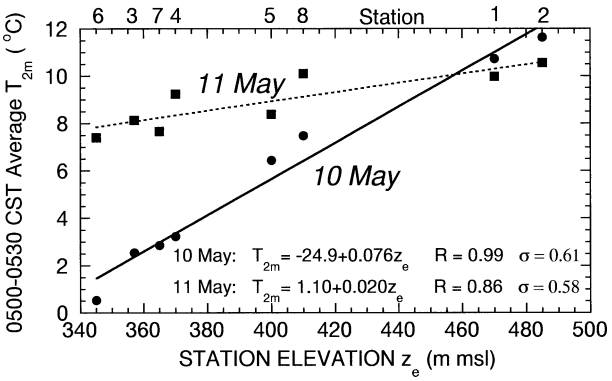

FIG. 3. Linear dependence of 30-min-averaged 2-m temperature on elevation, for temperature just before sunrise. Stations are labeled by number on top axis. For location of stations, see Fig. 1.

[1] We have broadened the range of values from the 1–2 h quoted in the abstract of AF, since we found maximum variability up to 3 h after sunset in some of the figures in the paper.

Unauthenticated | Downloaded 08/01/21 08:40 PM UTC

TABLE 1. Terrain characteristics for previous studies showing linear variation of nighttime surface air temperature with elevation.*

Authors	Elevation range for terrain (m)	Elevation range for observations (m)	Observation domain
Laughlin and Kalma (1987, 1990)	300	160	11 km × 11 km; one major drainage
Hocevar and Martsolf (1971)	350	275	16-km transects across valley
Harrison (1971)	180	150	13 km × 16 km; complex, three ridges
Acevedo and Fitzjarrald (2001)	130	118	15 km × 27 km; complex, three river valleys
Present study	150	150	30 km × 55 km; single watershed

* With the exception of Acevedo and Fitzjarrald (2001), the studies refer to minimum temperatures or temperatures shortly before sunrise.

steeper than the slope for the present case (~0.003–0.004).

The predawn focus of previous studies documenting the linear increase of temperature with terrain elevation could reflect the time after sunset needed to develop such patterns fully, as well as concern about killing frosts. Typically, as illustrated in Fig. 2, horizontal variability starts increasing rapidly around sunset; but after some time, it reaches a maximum or increases more slowly. Acevedo and Fitzjarrald (2001) note that local effects (vertical divergence of radiation and vertical heat flux) increase horizontal variability in temperature starting around sunset in response to surface heterogeneity; but horizontal advection eventually dominates, decreasing this variability. The timing of maximum horizontal variability varies. Looking at data from the Oklahoma Mesonet and the Little Washita Micronet, Fiebrich and Crawford (2001) report maximum horizontal variability not long after sunset. However, for nights where radiative cooling and drainage flows dominate, horizontal variability reaches a maximum 1–3 h after sunset in AF, and about 6 h after sunset on a night documented in the Little Washita Micronet by Fiebrich and Crawford. Figure 4 in Mahrt et al. (2001) shows that the horizontal temperature variation stops increasing significantly only ~1 h after sunset for a local gully flow.

In what follows, we use potential temperature Θ_{2m} rather than temperature, refer to the linear dependence of Θ_{2m} on elevation as $\Theta_{,ze} \equiv \partial\Theta_{2m}/\partial z_e$, and refer to the corresponding least squares best-fit line as the $\Theta_{,ze}$ line. For $\Theta_{,ze}$ equal to a constant value other than zero and a perfect linear fit, Θ_{2m} isopleths are parallel to the terrain contours. We will show that $\Theta_{,ze}$ is related to the thermal stratification $\Theta_{,z} \equiv \partial\Theta/\partial z$, where z is height. The relationship of $\Theta_{,ze}$ to the horizontal potential temperature gradient should be weak, since the stations used (1–8) are not lined up according to elevation (Fig. 1) except for the two highest stations being to the east of the remaining six.

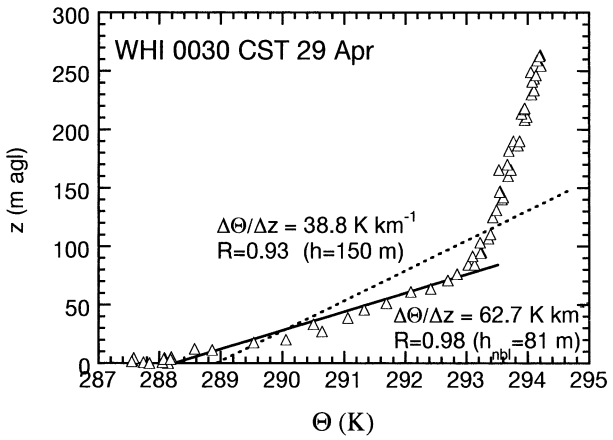

FIG. 4. Estimation of $\Theta_{,z}$ from radiosonde data. The kink in the profile marks the top of the NBL as defined here. Solid line is the least squares best-fit line for $\Theta_{,z}$ over NBL depth; dotted line is the best-fit line for $\Theta_{,z}$ over 150 m.

The outline of the paper is as follows. We describe the measurements in section 2, and the data-analysis procedure in section 3. For the presunrise hours, section 4 shows that Θ_{2m} varies linearly with station elevation ($\Theta_{,ze}$ = const) to good approximation, describes the behavior of the 10-m wind for the largest (>40 K m^{-1}) and smallest (near zero) values of $\Theta_{,ze}$, analyzes the relationship of $\Theta_{,ze}$ to $\Theta_{,z}$ and the Froude number Fr $\equiv S/Nh$, and relates the departures of Θ_{2m} from the $\Theta_{,ze}$ line at selected sites to surface cover and local terrain. Section 5 follows the development of the horizontal Θ_{2m} pattern through the night, showing that the timing of the maximum horizontal variability is a function of $\Theta_{,ze}$, and by inference, $\Theta_{,z}$ and the Froude number. In this section, we also relate the timing of the maximum horizontal Θ_{2m} variability under drainage-flow conditions to the scale of the terrain elevation, observation strategy, and surface cover. We propose a physical explanation for some of the observed behavior in section 6. The summary and conclusions appear in section 7.

2. Data

The fair-weather portion of CASES-97 (LeMone et al. 2000) was conducted from 21 April to 21 May 1997, to study the influence of the surface on the diurnal evolution of the boundary layer and how it varies horizontally, to provide a dataset for testing of land surface and boundary layer models, and to help design measurements in the region over longer timescales. The experimental array (Fig. 1) coincides with a roughly equilateral triangle outlining the southern edge of the Walnut River watershed. The wind-profiling systems at the vertices of the triangle (Whitewater, Beaumont, and Oxford) and the surface station at site 10 (Smileyberg) are

Unauthenticated | Downloaded 08/01/21 08:40 PM UTC

long-term installations that are part of the Atmospheric Boundary Layer Experiments (ABLE) array, operated by Argonne National Laboratory. Each ABLE wind-profiling system consists of a 915-MHz radar wind profiler, a Doppler minisodar, and a surface weather observing station, which obtains winds at 10 m (at the time of the experiment, the Whitewater surface station had not yet been installed). During CASES-97, surface-calibration instruments for the National Center for Atmospheric Research (NCAR) Cross-Chain Loran Sounding System (CLASS) radiosonde sites, which were collocated with the ABLE wind-profiling sites, provided wind measurements at 3 m. The estimated accuracy for the profiler winds is $\sim$1 m s^{-1}; this is probably an overestimate since different volumes were sampled for intercomparisons (Martner et al. 1993; Angevine and MacPherson 1995; Angevine et al. 1998). Uncertainties[2] for the Doppler sodars are $<$1 m s^{-1}.

The numbers in Fig. 1 denote the locations of surface flux/weather stations; here we focus on the eight NCAR stations, numbered 1–8. Temperatures were measured using Vaisala 50Y platinum resistance thermometers at 2 m above ground level (agl). While the absolute accuracy of these sensors is of the order of 0.03–0.05 K in the laboratory (T. Horst 2001, personal communication), additional error in the field results from radiative effects. In CASES-97, this error was minimized by putting each thermometer in a tube aspirated by a small pump. However, at winds over 2–3 m s^{-1}, the dynamic pressure deficit at the end of the tube was sufficient to keep air from being drawn past the sensor. Given similar winds at the stations (to be discussed later), the estimated error between the stations is of the order of 0.1 K. Winds were sampled with propeller vanes at 10 m, and with sonic anemometers at heights between 2 and 4 m. The propeller vanes respond well to winds $>\sim$1 m s^{-1}, while the sonic winds are accurate to $<$0.1 m s^{-1}.

Measurements from the surface towers and wind-profiling systems were taken continuously, but radiosonde observations were concentrated during intensive observing periods (IOPs), which were conducted during periods with slow changes in synoptic forcing and generally clear skies. During most IOPs, NCAR CLASS radiosondes were released from the three ABLE wind-profiling sites stations (WHI, BEA, and OXF in Fig. 1) at 90-min intervals between 0500 and 0330 CST the following day. The CLASS system used Vaisala sondes, and had reference readings of wind, temperature, pressure and humidity from a 3-m tower adjacent to the balloon-release site. The sounding operators were instructed to expose each sonde to the air by swinging it in a pendulum motion for 30–60 s, to allow equilibration with the environment; and to aim for a balloon rise rate of 5 m s^{-1}.

3. Analysis procedure

The surface data used in this study are half-hour averages, centered at 15 and 45 min past the hour. For comparison to sonde data, we used averages for the half hour following sonde release. Data were screened to eliminate nights with rain or passage of a front or wind-shift line through the array. For the remaining half-hour periods, Θ_{2m} values from the eight surface stations were then subjected to a least squares linear fit with z_e as the independent variable to obtain $\Theta_{,ze}$. We did not evaluate $\Theta_{,ze}$ if more than one station had bad data.

The thermal stratification $\Theta_{,z}$ is based on a least squares linear fit to hand-edited 1.5-s-resolution radiosonde potential temperature as a function of altitude, using data from the surface to either $h = 150$ m or the nocturnal boundary layer (NBL) depth. As previously noted, h is the altitude range of the surface flux stations and also a measure of the range in terrain elevation. We define the NBL depth at each wind-profiling site as the height at which $\Theta_{,z}$ from the collocated radiosonde sounding abruptly becomes smaller (Fig. 4), so the air within the NBL is not necessarily turbulent.

Here, we define the Froude number by

$$\mathrm{Fr} = \frac{S}{Nh}, \tag{1}$$

where S and N are averaged between the surface and h; Fr is calculated separately for Beaumont, Oxford, and Whitewater for each nighttime radiosonde release time, using wind data from the radar wind profilers, sodars, surface towers, and thermodynamic data from the radiosondes. The wind components from the profiling systems are roughly 1-h averages, interpolated to a common time (in this case on the hour or 30 min past the hour to coincide with the radiosonde soundings). We calculate S primarily from the Doppler minisodar and tower data, since usable 915-MHz radar winds start around 150 m above the surface. Similarly, the Doppler minisodar data are unreliable below 25 m, so the winds at that level are found by interpolating linearly between the minisodar winds at 25 m and the tower winds at 10 m (ABLE) or 3 m (NCAR CLASS). Finally, the resulting wind data are subjected to a linear fit, interpolated to 5-m intervals, and then averaged. We base N on a least-squares linear fit of hand-edited 1.5-s-resolution radiosonde virtual temperature as a function of altitude, using data between the surface and h.

4. Results—The last few hours before sunrise

a. General behavior

The data in Fig. 5 show that the linear relationship between Θ_{2m} and z_e in the last hours before sunrise is

[2] From R. L. Coulter (2002, personal communication). Based on 1 yr of comparisons with tower data, the bias for $U = -0.20 \pm 0.84$, for $V = -0.20 \pm 0.98$, with the negative values possibly due to counting Doppler minisodar data down to 10 m. For further evaluation of Doppler minisodar data, see Coulter and Martin (1986).

Unauthenticated | Downloaded 08/01/21 08:40 PM UTC

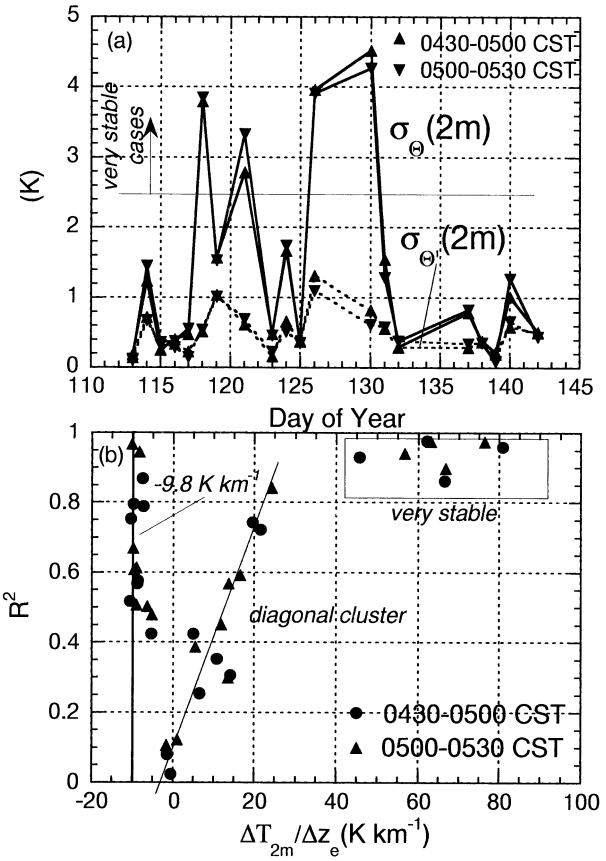

FIG. 5. Measures of the robustness of the least squares linear relationship between z_e and Θ_{2m} for the last two complete half-hour periods before sunrise. (a) Spatial standard deviation of Θ_{2m} relative to the mean (σ_Θ), and the standard deviation relative to the $\Theta_{,ze}$ line ($\sigma_{\Theta'}$) for days in CASES-97 with no precipitation, fronts, or wind-shift lines; (b) square of the correlation coefficient R between z_e and T_{2m} as a function of the z_e–T_{2m} regression line slope $\Delta T_{2m}/\Delta z_e$. Heavy vertical line indicates adiabatic lapse rate.

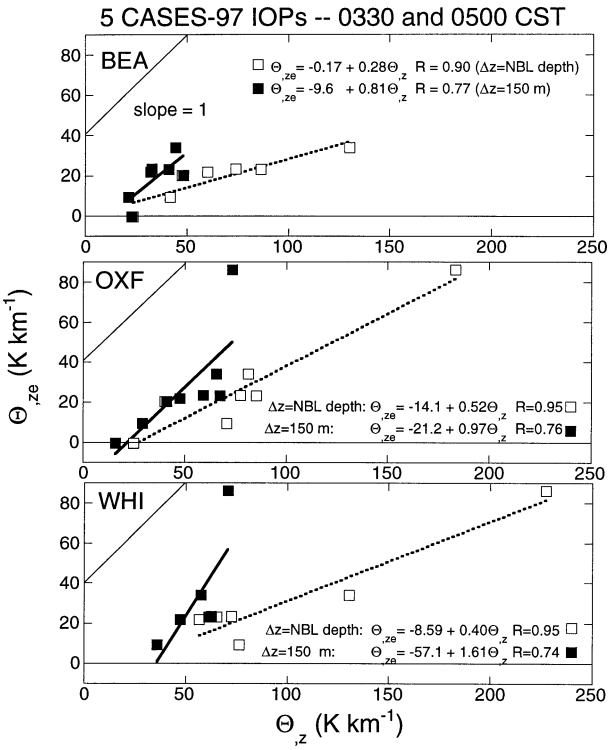

FIG. 6. Change of Θ_{2m} with elevation $\Theta_{,ze} \equiv \partial\Theta_{2m}/\partial z_e$ as a function of thermal stratification $\Theta_{,z} \equiv \partial\Theta/\partial z$ based on rawinsonde data at 0330 and 0500 CST and surface data for the half-hour periods centered at 0345 and 0515 CST. Solid line is $\Theta_{,z}$ estimated through the lowest 150 m; dotted line is $\Theta_{,z}$ estimated through the depth of the NBL; $\Theta_{,z}$ is calculated using radiosonde data from Beaumont (top), Oxford (middle), and Whitewater (bottom). Each point represents both good soundings and 7 or 8 stations with good temperature data. A line with slope of 1 appears in the upper left corner of each frame.

valid to good approximation, especially for the nights with $T_{,ze} > 40$ K km^{-1}. We use T_{2m} instead of Θ_{2m} in Fig. 5b because there are many instances for which $\Delta T_{2m}/\Delta z_e$ is equal to the adiabatic lapse rate, for which there would be zero correlation between Θ_{2m} and z_e. From Fig. 5a, we see that $\sigma_{\Theta'}$, the standard deviation relative to the $\Theta_{,ze}$ line, is usually of the order of 0.5 K, comparable to those for the examples in Fig. 3. The four nights with large spatial standard deviations relative to the mean (σ_Θ) are also the four nights with the largest values of $\Delta T_{2m}/\Delta z_e$ and therefore $\Theta_{,ze}$. The regression lines for these four nights explain more than 85% of the variance ($100R^2$, Fig. 5b). At the other extreme, in Fig. 5b are several nights with $-\Delta T_{2m}/\Delta z_e = 9.8$ K km^{-1}, the adiabatic lapse rate, and varying values of R^2. For these nights, the two standard deviations ($\sigma_{\Theta'}$ and σ_Θ) in Fig. 5a are nearly equal, and sometimes quite small. The nights with intermediate values of $\Delta T_{2m}/\Delta z_e$ form a diagonal cluster of points in Fig. 5b, for which $\Delta T_{2m}/\Delta z_e$ and the variance explained by the $T_{,ze}$ line increase together. From Fig. 5a, $\sigma_{\Theta'}$ for these days varies, with values up to ~1 K.

Figure 6 relates $\Theta_{,ze}$ to $\Theta_{,z}$ obtained from radiosonde data for the five IOPs, for the last two release times before sunrise (~0530–0600 CST). We calculate $\Theta_{,z}$ for each wind-profiling site separately. From the figure, $\Theta_{,z} > \Theta_{,ze}$ if $\Theta_{,z}$ is evaluated over the NBL depth (often much less than 150 m), and $\Theta_{,z} \sim \Theta_{,ze}$ if $\Theta_{,z}$ is calculated over the elevation range of the surface stations (150 m). Larger Θ_{2m} increases with elevation are associated with greater thermal stratification, and thermal stratification is close to static stability in this relatively dry environment. Thus, we label non-IOP nights (no radiosonde data to determine $\Theta_{,z}$) with large $\Theta_{,ze}$ as ''very stable'' cases. As has often been documented, the very stable cases correspond to clear skies and light winds, while the less stable cases correspond to more clouds or wind. The lower correlations between $\Theta_{,ze}$ and $\Theta_{,z}$ evaluated over 150 m probably relate to a less-robust linear fit to the radiosonde data that results from the change in slope of the Θ profile at the top of the NBL (Fig. 4).

Surprisingly, the $\Theta_{,z}$–$\Theta_{,ze}$ best-fit lines in Fig. 6 cross the $\Theta_{,z}$ axis at $\Theta_{,z} > 0$. Figures 5 and 7 show that near-

Unauthenticated | Downloaded 08/01/21 08:40 PM UTC

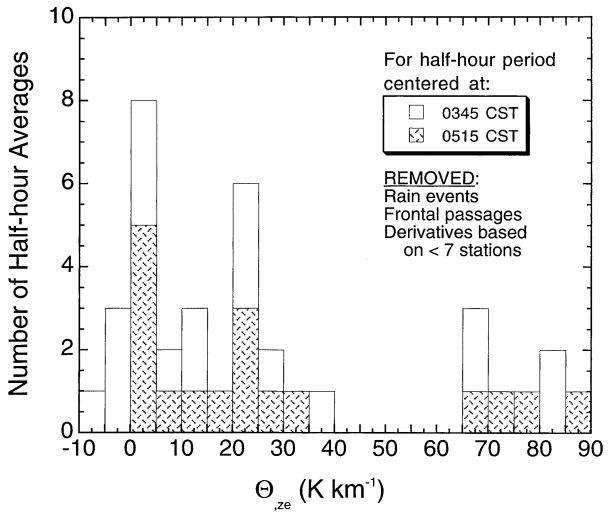

FIG. 7. Distribution of $\Theta_{,ze}$ for undisturbed 0330–0400 and 0500–0530 CST periods during the entire field program.

zero values of $\Theta_{,ze}$ are common during the predawn hours. In Fig. 7, $\Theta_{,ze} \sim 0$ for 11 or roughly one-third of the half-hour periods. When soundings are available for such events (a total of six documented, including the one represented in the top frames of Fig. 6), $\Theta_{,z} > 0$ through the depth of the NBL and through the lowest 150 m. That is, in many instances, Θ_{2m} *does not vary with elevation even though static stability is positive.* A constant value of Θ_{2m} is consistent with near-surface air following the terrain dry adiabatically. We will show in section 4b that the near-surface flow is coupled to the ambient flow, but that Θ_{2m} is constant because it changes everywhere at the same rate under these conditions. We argue in section 6 that the latter behavior is consistent with flow coupled to the surface.

b. Behavior of flow for the extreme values of $\Theta_{,ze}$

When $\Theta_{2m} = \text{const}(\Theta_{,ze} \approx 0)$, the flow at 10 m is coupled to the ambient wind. The wind direction at 10 m is consistent with the ambient wind at Beaumont, if one allows for the change of wind direction with height, and the wind direction change with z_e at the eight stations is small, with a median value of 7.5° over 150 m. Averaged over 9 days with $\Theta_{2m} = \text{const}$ over the half-hour period 0500–0530 CST, the wind components U (positive east) and V (positive north) and the wind speeds all increase linearly with elevation (Fig. 8a). As in the case of Θ_{2m}, these three quantities vary linearly with elevation to good approximation on individual days as well. Comparing the individual days, the greater increases in speed S with elevation are associated with greater wind speeds, with $\partial S/\partial z_e$ roughly doubling for each doubling of S.

A schematic of the flow appears in Fig. 9a. The near-surface Θ surfaces are depicted as farther apart with lower wind speeds, as implied from mass continuity, provided the flow is two-dimensional and isentropic. However, the small number of $\Theta_{,ze} \approx 0$ events with radiosonde data do not show a clear relationship between $\Theta_{,z}$ and location in the watershed. The streamlines above 10 m are drawn to be consistent with linear solutions for flow over low hills (e.g., Belcher and Wood 1996).

For $\Theta_{,ze} \sim 0$, and air parcels moving along the terrain surface with the ambient wind, we might expect the flow to be dry adiabatic. Instead, Θ_{2m} changes uniformly across the array, at rates varying from -1.34 to $+0.32$ K h^{-1}. Wind directions on some nights suggest Θ_{2m} changes consistent with warm- or cold-air advection (keeping open the possibility for dry-adiabatic flow), but there are also nights with warming and north winds, and cooling with south winds (consistent with diabatic processes). We argue in section 6 that uniform temperature changes, like adiabatic flow, are consistent with the surface layer being coupled to the ambient wind.

The winds for the very stable cases with large values of $\Theta_{,ze}$ show an entirely different pattern. Figure 8b shows the dependence of U, V, and wind direction on station elevation for the same time interval as Fig. 8a but for days with $\Theta_{,ze} > 40$ K km^{-1}. The Doppler wind profilers and Doppler minisodars show ambient winds from the south on all 4 days, with a slight easterly component on all days except for day 121, consistent with the winds at the highest site (station 2). The 10-m winds at lower elevations have an easterly component on all 4 days, implying a drainage flow down the long, gentle slope on the east side of the Walnut River (Fig. 1) that is reinforced by ambient wind on 3 days. The easterly flow reaches a weak maximum of $\sim$2 m s^{-1} at station 8 (410-m elevation), and then slows considerably at lower elevations. Surprisingly, the wind at station 5 on the west side of the river (Fig. 1) also has an easterly component, as does the 10-m wind at Oxford (not shown). The wind at elevations greater than $\sim$370–400 m has a southerly component, consistent with the ambient wind, but there is down-valley flow (from the north) at lower elevations, except for station 6, which lies to the south (Fig. 1).

The observed wind pattern is consistent with a stable cold pool, isolating the surface air at elevations below 370–400 m from the air above, as shown in the schematic in Fig. 8b. The pool drains southward, but becomes stalled north of station 6. This scenario is supported by the north winds and the much weaker east winds below 370 m. Further, the decrease in east wind between stations 8 and 4, which is evident for the 3 days with complete data, is consistent with downslope easterly flow encountering and then flowing over the denser cold pool (e.g., Atkinson 1995; Banta and Gannon 1995) to station 5. In the absence of a cold pool, we would expect the easterly flow to remain steady or even reach a maximum at the bottom of the watershed, as suggested by the model results of Bossert and Poulos

Unauthenticated | Downloaded 08/01/21 08:40 PM UTC

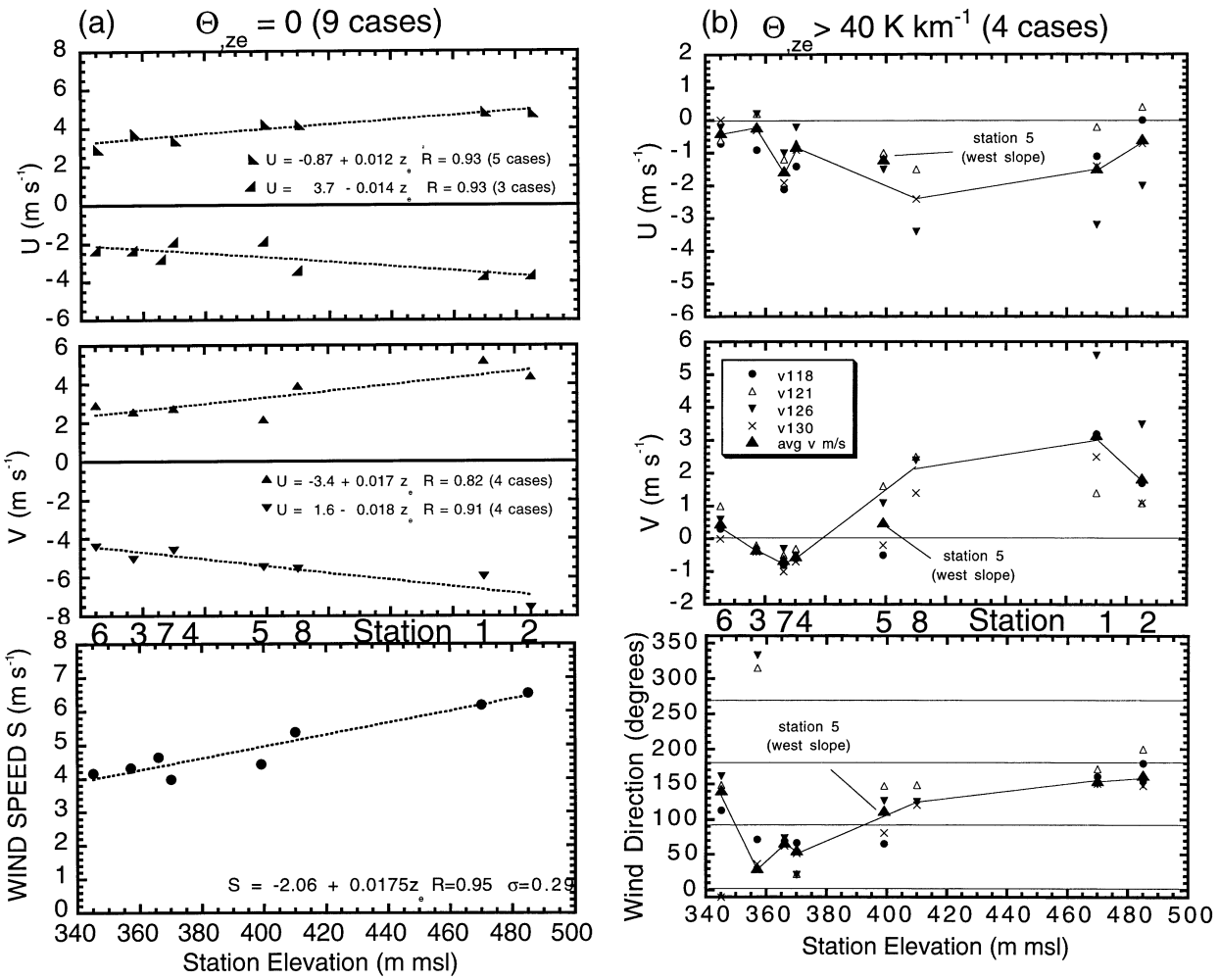

FIG. 8. Relationship of 30-min-averaged winds at 10 m to elevation at 0500–0530 CST for (a) $\Theta_{,ze} \approx 0 (\Theta_{2m} = \text{constant})$ with dotted line the least squares best-fit line as a function of z_e; and (b) $\Theta_{,ze} > 40$ K km^{-1}, with solid lines connecting the stations on the eastern side of the Walnut River. In (a), wind components of the same sign are combined, and cases wind components varying around zero were not included, reducing the number of component averages from 9 to 8.

(1995). This model does not deal with the effects of a competing drainage flow from the other side of the valley. However, the flow down the eastern side of the Walnut River Watershed, which is 3 times as broad as the western side and has the same slope, should dominate. Furthermore, the ambient flow had an eastern component on 3 days, reinforcing the drainage flow down the eastern slope and possibly eliminating the drainage flow down the western slope (e.g., Coulter et al. 1989).

There are several indications that the cold-pool top is between 370 and 400 m. There is a subtle change in the slope of the temperature gradient around 400 m at stations 5 and 8 in Fig. 3 for 10 May (day 130) that becomes more convincing if we average the 3 days with temperatures from all eight stations as shown in Fig. 10. The western border of the watershed lies at 380–410-m elevation at the latitudes of all surface stations except for station 6, providing an upper limit for cold-pool depth. The edge of the watershed drops southward, reaching an elevation of 360 m near Oxford, and potentially warmer air above Oxford on some nights is consistent with the top of the cold pool descending southward with the terrain. The calm to south winds at station 6 (345-m elevation) indicates that the cold pool does not reach that far south. This suggests that the south winds, observed on all four nights, are strong enough to keep the cold pool from spilling out of the watershed.

It is noteworthy that the departure from a linear Θ_{2m}–z_e relationship is relatively minor despite the presence of the cold pool. We suggest two interpretations. First, the eastern slope of the watershed changes little enough that the processes determining the temperature variation within the cold pool are similar enough to those at higher elevations to create a similar dependence of Θ_{2m} on elevation. And second, some of the surface flow continues down into the river basin, but is retarded by the stable stratification.

Unauthenticated | Downloaded 08/01/21 08:40 PM UTC

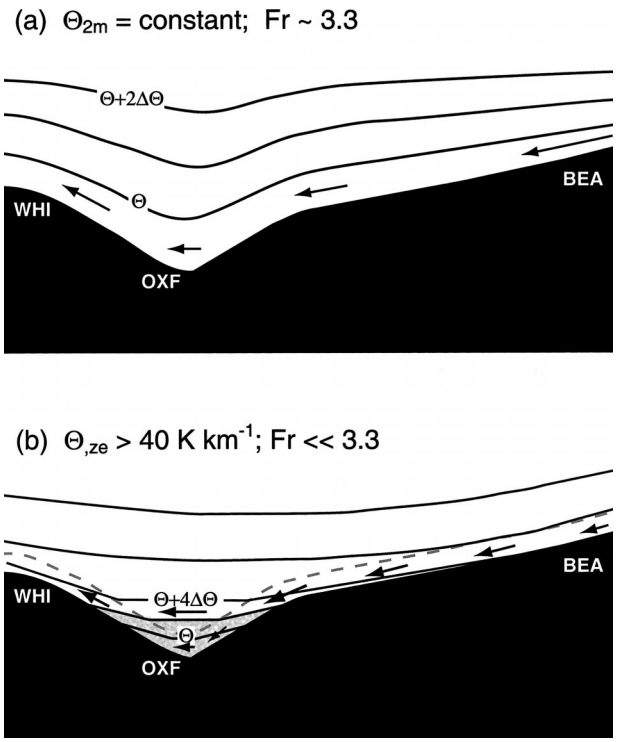

FIG. 9. Schematic east–west cross section of wind and potential temperature distribution across the watershed at latitudes of the surface stations for (a) constant Θ_{2m} but stable thermal stratification (Fr $\sim$ 3.3) and (b) $\Theta_{,ze} > 40$ K km^{-1}(Fr $\ll$ 3.3). WHI, OXF, and BEA show rough locations of ABLE wind-profiling systems with respect to the sides of the watershed. Vertical coordinate is exaggerated to emphasize temperature stratification near the ground; dashed line in (b) is at 10 m AGL. Shading shows southward-flowing cold pool.

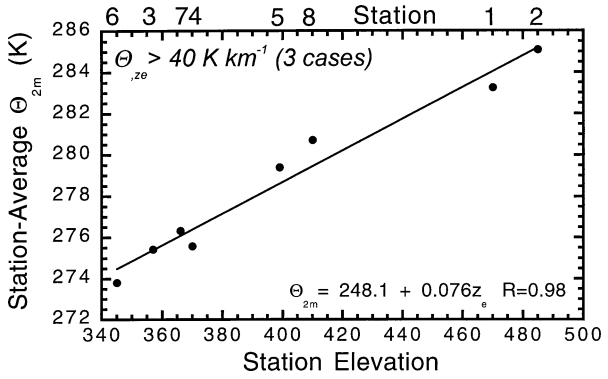

FIG. 10. For the 3 days with $\Theta_{,ze} \gg 40$ K km^{-1} and temperatures at all eight surface stations at 0430–0500 CST, average Θ_{2m} as a function of elevation. The solid line and equation correspond to the least squares best-fit line to the eight points.

The low-speed drainage winds associated with the four stable cases are half-hour averages. On all 4 days, however, the 5-min maximum gust data, available at 10 m at stations 1–6, are consistent with low-speed flow with fluctuations of the order of 1 m s^{-1}, some of which could be associated with the response of the propeller vanes. The drainage current in shallow terrain documented by Mahrt and Larsen (1982) was similar, with light winds that remained relatively steady with a few weak pulses after the initial ''surge'' with a speed of 2 m s^{-1}. Model results (e.g., Atkinson 1995) also associate low-speed drainage winds with shallow slopes. Other studies in the Walnut River watershed have focused on the strong fluctuations associated with density currents (surges of cold air), but these seem to be relatively rare. The density current observed in the Walnut River watershed in an earlier field experiment by Blumen et al. (1999), was the only one observed that night, and the few density currents that did occur on other nights when weather conditions seemed favorable, were relatively weak. Similarly, there were surprisingly few density currents detected during CASES-99 (W. Blumen and J. Lundquist 2002, personal communication; Poulos et al. 2002), even though there was more than enough instrumentation to document them (e.g., Sun et al. 2002).

c. Dependence of flow on Froude number

The thermal stratification ($\sim\Theta_{,ze}$) separates nights with flow coupled to the surface from nights with drainage flows, and the nights with coupled flow have stronger winds. Thus, we examine the relationship of $\Theta_{,ze}$ to Fr as defined by (1). We use h = 150 m, roughly the range of station elevations and elevations in the lower watershed. The results appear in Fig. 11. The intercept, where $\Theta_{,ze} = 0$ or Θ_{2m} is independent of elevation, occurs at ln (Fr) = 1.2, which corresponds to Fr = 3.3.[3] Taking the radiosonde stations separately, the Oxford (360-m elevation) and Whitewater (420-m elevation) yield slightly lower values (ln Fr $\sim$ 1.1; Fr $\sim$ 3 for both), with Beaumont (478-m elevation) remaining about the same, consistent with the expectation of stronger winds at higher elevations. Our value of Fr $\sim$ 3.3 is slightly higher than the Fr = 2 value that Mason (1987) and Holdon et al. (2000) require for air to flow up and down the terrain with the ambient wind. However, the two values are remarkably similar given the differences between the slopes (0.2–0.3) of the terrain those authors dealt with and the present case (0.003–0.004), and differences in the way Fr was computed.

Use of a Froude number carries with it the implication that the air has enough momentum to overcome the unfavorable stable stratification to force air over the top of hills and down into valleys. Mason (1987) has couched this process in terms of pressure gradients or potential and kinetic energy. An alternative physical in-

[3] An earlier calculation using gradients over the NBL depth and U from radiosondes also yielded a straight line [$\Theta_{,ze} = 45.7 - 17.3$ ln(Fr), $R = 0.91$] with an intercept of ln(Fr) = 2.84 (LeMone and Grossman 2000) that changed little when the two points with large $\Theta_{,ze}$ were eliminated. Using only 0500 CST soundings does not significantly affect the best-fit line.

Unauthenticated | Downloaded 08/01/21 08:40 PM UTC

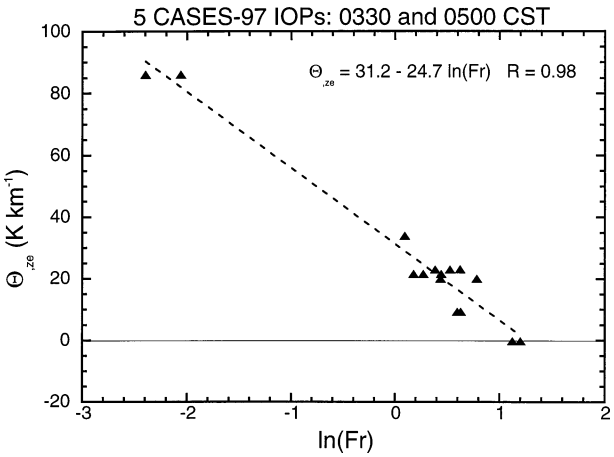

FIG. 11. Relationship of the natural logarithm of the Froude number $S/(Nh)$ to $\Theta_{,ze}$ for 0330 and 0500 CST. Eliminating the two extreme points leads to the line $\Theta_{,ze} = 32.0 - 26.0$ ln Fr. Both lines intersect the ln Fr axis at ln Fr = 1.2.

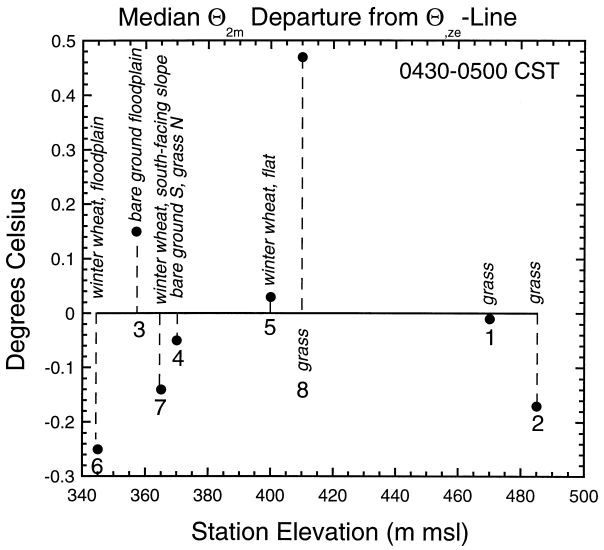

FIG. 12. For undisturbed nights in CASES-97, the median Θ_{2m} departure from the $\Theta_{,ze}$ line based on data from 0430–0500 CST.

terpretation is that strong winds or weak vertical stratification can promote enough vertical mixing to couple the surface layer to the ambient wind. From (1),

$$\mathrm{Fr}^2 \equiv \frac{S^2 h^{-2}}{\dfrac{g}{\Theta_v}\dfrac{\partial \Theta_v}{\partial z}} \approx \frac{1}{\mathrm{Ri}}, \tag{2}$$

provided h is a constant. Holden et al. (2000) note a general relationship similar to (2), but point out that Ri, and hence coupling between the surface and ambient wind, can very over complex terrain.

d. Departure of Θ_{2m} from the z_e–Θ_{2m} regression line ($\Theta_{,ze}$ line)

Examination of plots of z_e versus Θ_{2m} for the last hours before sunrise reveals that Θ_{2m} at certain stations tends to be warmer or cooler than the $\Theta_{,ze}$ line. The median departures from the $\Theta_{,ze}$ line for the period 0430–0500 CST are plotted as a function of station elevation in Fig. 12. We have already discussed the kink in the Θ_{2m} profile at around 390–410 m in Fig. 10, which is associated with warm departures for stations 8 and 5, and which could be related to the presence of a cold pool. Other possible factors influencing such departures are (a) temperature-sensor bias; (b) local drainage flows, as suggested by Laughlin and Kalma (1990);[4] (c) land cover (Cornford 1938; Oke 1987, p. 234; AF); and (d) soil moisture (Banta and Gannon 1995). The flux stations were located in remote and nearly flat areas with at least a 100-m fetch in all directions, so there was neither sheltering from nearby trees or structures nor mixing from passing motor vehicles to influence local cooling.

To isolate the local factors influencing the temperature departures, we plot the Θ_{2m} departure from the $\Theta_{,ze}$ line corresponding to the half-hour average wind vector for three stations, and show the corresponding terrain centered at each site (Fig. 13). We compare stations 3 and 6 because they have different ground cover but are at similar elevations. This avoids the comparison being too dependent on the linear fit. Station 4 is shown because the fetch depends on wind direction. We use winds from the sonic anemometers because they are at 3–4 m, closer to the level of the temperature sensor and more likely to feel the effect of shallow drainage currents from nearby terrain features. The wind vectors are similar for each day for the station pairs, so differences in the ventilation

[4] Mahrt and Heald (1983) inferred similar behavior based on radiometric surface temperatures from aircraft measurements over uneven terrain.

→

FIG. 13. For time periods of Fig. 12, (left) the Θ_{2m} departure at three stations from the $\Theta_{,ze}$ line as a function of wind velocity and station. Stations 3 (345 m MSL) and 6 (357 m MSL) are at similar elevations; the fetch at station 4 is a function of wind direction. Each temperature is labeled with the corresponding Julian day. For example, 119 is 29 Apr, 130 is 10 May, and 140 is 20 May. Departures ≤0.1 K are in the noise. (right) Surrounding terrain, based on U.S. Geological Survey 7.5-min topographic maps. Frames are 3 km × 3 km; contour interval is 10 ft (3.05 m).

Unauthenticated | Downloaded 08/01/21 08:40 PM UTC

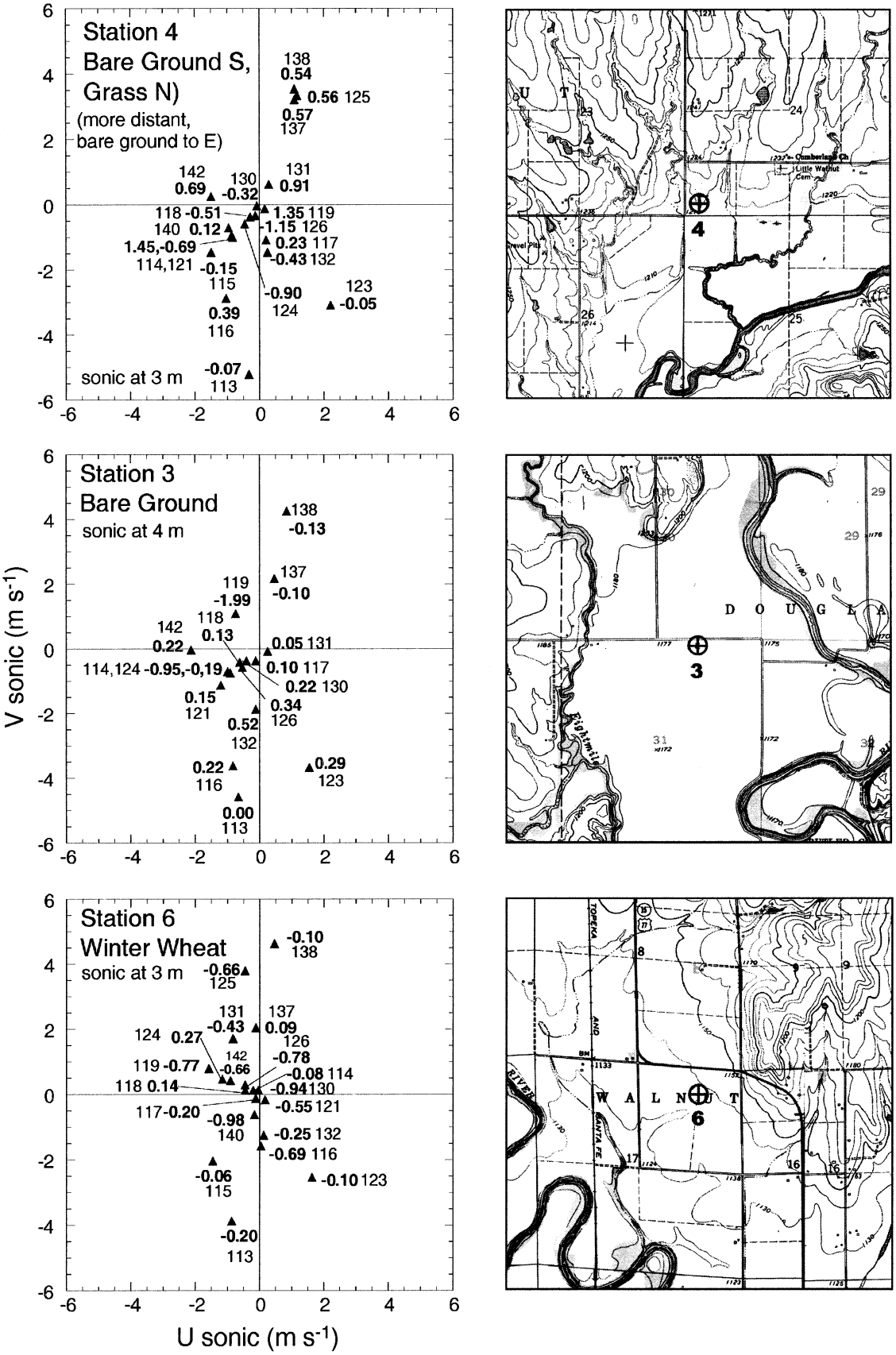

Unauthenticated | Downloaded 08/01/21 08:40 PM UTC

of the temperature sensors should contribute little to differences in their temperatures.

From Fig. 12, station 6 (winter wheat) tends to be cooler than predicted by the $\Theta_{,ze}$ line, and station 3 (bare ground) tends to be warmer. We attribute these departures primarily to the effects of the surface cover. First, the height of the winter wheat increases from 0.46 m on 19 April to 0.61 m on 5 May, to a maximum of 0.92 m on 12 May, leading to a zero-plane displacement height d increasing from 0.32 to 0.64 m, assuming d is 70% of the crop height (e.g., Campbell and Norman 2000). Both the stable boundary layer flux-profile relationship in Businger et al. (1971) and a logarithmic temperature profile suggest cool biases ranging from 0.06 to 0.2 K resulting from the temperature sensor being 1.36 m rather than 2 m above the effective surface at the winter wheat site for the mainly less-stable days for which all relevant data are available. This is probably an underestimate: for the period 0300–0600 CST, G. Poulos (2002, personal communication) finds the average temperature at 1.36 m is ~0.5 K cooler than that at 2 m on the 60-m tower in CASES-99, which had mostly clear skies or high clouds at night. The coolest vegetation-induced temperature departures from expected values found by Cornford (1938), whose measurements were 3 ft (0.9 m) above the ground, were over tall grass, suggesting a role of displacement height: indeed one figure shows an isotherm following the vegetation height. Second, the winter wheat acts as mulch, insulating the ground from the cooling air, so that the air receives less heat from the soil compared to the bare-ground site (e.g., Oke 1987, p. 234).

The influence of the local terrain on the Θ_{2m} departures is unclear, because when there is flow from the nearby bluffs on light-wind nights, it is from the same direction as the watershed-scale flow. At station 6, there is preference for flow with an easterly component on light-wind nights, suggesting flow at least reinforced by drainage from the bluffs to the east of the station. Of the 13 days with an easterly wind component, 7 have significant ($>$0.1 K) negative departures from the $\Theta_{,ze}$ line. At station 3, two of the three significant cold departures, that is, days 114 and 124 or 24 April and 4 May, occur with north winds, which are associated with down-valley flow possibly reinforced by drainage from the bluffs to the north. Comparing the wind at 10 and 2–3 m, the 10-m wind is typically slightly stronger, as might be expected for the valley-scale flow. The anomalous cool departure with a south wind on day 119 (29 April) at station 3 could be related to a subsynoptic wind-shift line that passed through the western part of the array, lowering the temperature at some of the stations. It is not know how common such disturbances are, since some of the ''synoptic'' events eliminated from the dataset could have been subsynoptic. A second subsynoptic wind-shift line passed through the array on 14 May (day 134), affecting all the stations and Wichita, leading us to exclude that day from the analysis.

Station 4 is on nearly flat terrain with a gentle south-facing slope, but the upstream vegetation is a function of wind direction (Fig. 13). All of the days with south wind component >1 m s^{-1} have positive Θ_{2m} departures >0.5 K, suggesting an effect of the bare ground just south of the site. All of the cool departures are associated with a north wind component (grass fetch) or nearly calm winds. It could be argued that both terrain (drainage winds) and surface cover contribute to the departures from the $\Theta_{,ze}$ line. The grass was considerably thinner than the winter wheat and grew from 7 to 15 cm during the experiment, and there was mostly bare ground with some stubble to the south. Thus, the zero-plane displacement probably did not play a significant role at station 4.

We conclude that vegetation and possibly local terrain lead to the Θ_{2m} departures from the $\Theta_{,ze}$ line, shown in Fig. 12. The displacement heights for the other winter wheat and grass sites are similar to those for stations 6 and 4, respectively, suggesting similar outcomes. We already associated the warm departures from the $\Theta_{,ze}$ line at stations 8 and 5 for the very stable cases with the presence of a cold pool. This could also apply to the intermediate-stability cases. It is likely that the winter wheat at station 5 keeps it cooler than station 8 (grass), but the station positions on opposite sides of the watershed could also play a role. We do not have sufficient data to assess the effects of soil moisture, which varied significantly during CASES-97 (LeMone et al. 2000). Our practice of siting the stations in broad, horizontally homogeneous areas may lessen the effects of local terrain.

5. Results—Development of the temperature pattern

From the foregoing, the CASES-97 data reveal a linear relationship of Θ_{2m} to elevation by the last hours before sunrise, in accordance with earlier studies. We find that $\Theta_{,ze}$ is related to both $\Theta_{,z}$ and the Froude number Fr, and that $\Theta_{,ze} \approx 0$ when Fr reaches a value of 3.3. In this section, we examine how the previously discussed relationships develop during the night as a function of ambient conditions.

In Fig. 14, the linear relationship between $\Theta_{,ze}$ and $\Theta_{,z}$ shows more scatter and has lower correlation for data through the night, compared to the last hours before sunrise (Fig. 6). Further, $\Theta_{,ze} \sim 0.5\Theta_{,z}$ averaged from the surface to 150 m, compared to $\Theta_{,ze} \sim \Theta_{,z}$ for the presunrise data. Similarly, the linear relationship between Froude number and $\Theta_{,ze}$ through the night is less robust, explaining only 65% of the variance ($R = 0.84$; Fig. 15), as opposed to about 96% of the variance for the early morning data ($R = 0.98$; Fig. 11). However, ln Fr $= 1.3$ (Fr $= 3.7$) for $\Theta_{,ze} \approx 0$, similar to the early morning value of 1.2.

The distribution in Fig. 16 shows a tendency for $\Theta_{,ze}$ to increase through the night. All but one of the cases

Unauthenticated | Downloaded 08/01/21 08:40 PM UTC

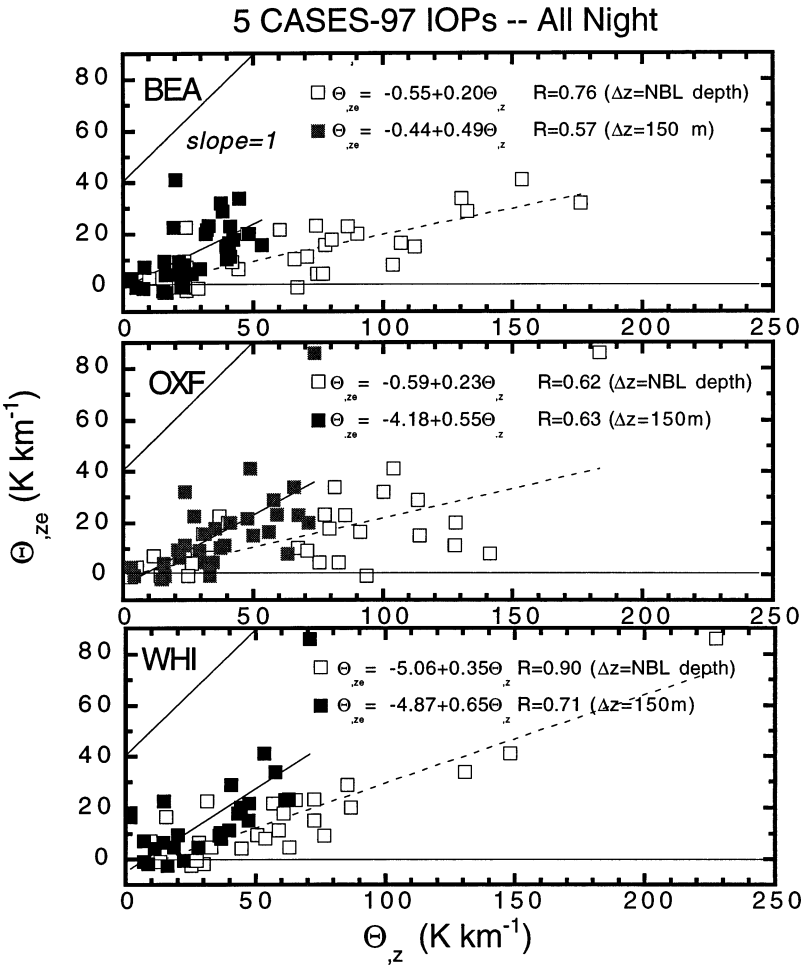

FIG. 14. As in Fig. 6, but for data from radiosonde data through the night (1830–0500 CST), and surface data half-hour averages at center times from 1845 to 0515 CST.

for which $\Theta_{,ze} \geq 60$ K km^{-1} occur after 2430 CST, with over half occurring after 0330 CST. Large negative values, which occur mostly in the early evening, are probably associated with local effects, which create large scatter and influence the slope of the $\Theta_{,ze}$, line, as will be seen below. There is a slightly larger fraction of half-hour periods with $\Theta_{,ze} \approx 0$ through the night (Fig. 16) than for the predawn hours (Fig. 7). Counting values within 5 K km^{-1}, $\Theta_{,ze} \approx 0$ for 28% of the half-hour averages in Fig. 7, and 32% in Fig. 16. Counting values within 10 K km^{-1} to allow for larger scatter, especially in the earlier hours of the evening, shows that $\Theta_{,ze} \approx 0$ 39% of the time in Fig. 7 and 50% of the time in Fig. 16.

Figure 17a shows the evolution of horizontal variability of Θ_{2m} for nights without rain, fronts, or windshift lines. The standard deviations with respect to both the spatial mean (σ_Θ) and the $\Theta_{,ze}$ line ($\sigma_{\Theta'}$) increase for the first 2 h after sunset. After this, σ_Θ stays roughly constant, but $\sigma_{\Theta'}$ decreases to a presunrise value largely related to local site characteristics, as shown in section 4d. This indicates that the linear relationship of Θ_{2m} to z_e is most robust just before sunrise. Thus, it is not surprising that the relationship of $\Theta_{,ze}$ to the Froude number and $\Theta_{,z}$ is most robust in the early morning hours.

The evolution in Fig. 17a represents a range of behaviors that relate to the value of $\Theta_{,ze}$ or Fr. For example, for the four cases with $\Theta_{,ze} > 40$ K km^{-1} at 0445 CST (Fig. 17b) and thus the lowest Fr (Fig. 11), σ_Θ increases rapidly for 6–8 h after sunset, and then slowly increases until sunrise. Much of the presunrise variability is watershed scale, as indicated by the decrease in $\sigma_{\Theta'}$ to a predawn minimum. This is consistent with the fact that the largest values of $\Theta_{,ze}$ tend to occur after 0045 CST (Fig. 16).

For the individual days represented in Fig. 17b, the lag time between sunset and maximum σ_Θ is 6.5–9 h, much longer than the 1–3 h of AF, and slightly longer on average than the 6 h for the night documented in Fiebrich and Crawford (2001) for clear nights with light winds. Acevedo and Fitzjarrald (2001) call this time the

Unauthenticated | Downloaded 08/01/21 08:40 PM UTC

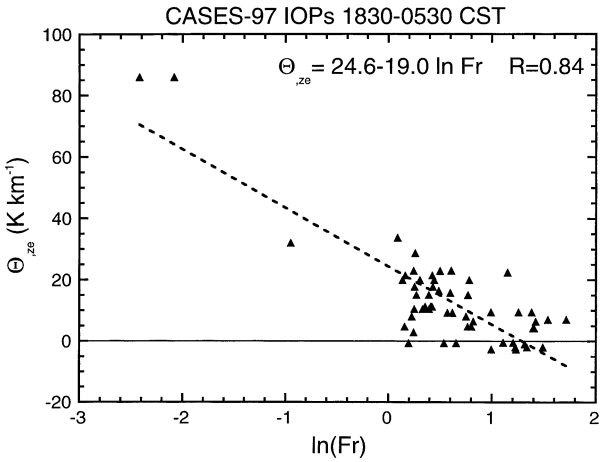

FIG. 15. As in Fig. 11, but for data through the night.

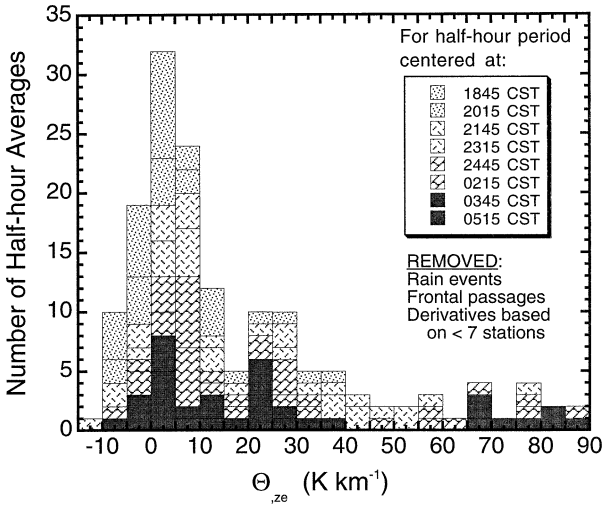

FIG. 16. As in Fig. 7, but through the night.

end of the boundary layer ''evening transition,'' which begins ½–1 h before sunset as a new stable layer starts forming at the surface. Acevedo and Fitzjarrald attribute the buildup of horizontal variability to heterogeneity and local processes (radiation and turbulence flux divergence) sensitive to that heterogeneity. These processes decouple the surface layer from the decaying residual boundary layer overhead. Areas sheltered from the wind by trees or terrain are particularly susceptible to decoupling. Businger (1973) notes that rapid radiative cooling at the surface within this newly isolated layer can develop the most stable stratification of the night [Mahrt et al. (1998, 2001) find this behavior to be common but not universal]. The layer remains decoupled until the horizontal pressure-gradient force increases the wind at the layer top and lowers the local Richardson number enough to reintroduce turbulent mixing (van de Wiel et al. 2002). With time, horizontal advection becomes relatively more important (e.g., AF; Mahrt et al. 2001), and smoothes out smaller-scale horizontal variability, lowering the horizontal standard deviation (AF).

We suggest that the typical time interval between sunset and maximum horizontal variability σ_Θ for CASES-97 low-Fr nights differs from that of AF and other studies primarily because of the scale of the terrain, the sampling strategy (station spacing, station exposure, and surface cover), with data-analysis strategy (time averaging) playing a secondary role. Figure 18 shows that the time between sunset and the transition from a rapid increase in σ_Θ to a stable value, as in Fig. 4 of Mahrt et al. (2001), or to a maximum value, as for the other studies depicted. The CASES-97 value is an average of the time delay for horizontal variability for the four very stable cases. For horizontal scale, we take the distance across the relevant watersheds (or airsheds). To obtain this scale for CASES-97, we use the distance across the part of the Walnut River watershed where the array is located (Fig. 1). Similarly, we use the distance across Little Washita River basin and a representative distance across the three river valleys in Fig. 3 of AF, while we determine the distance across the gully from Fig. 2 of Mahrt et al. (2001).

It is likely that the observed scale dependence in Fig. 18 is related to advection. The numerical simulation in AF shows that advection smoothes out horizontal variability on smaller scales, leading variability on the scale of the dominant terrain (in their simulation, ''terrain'' was only one scale). This is consistent with the decrease in standard deviation (small-scale variability) relative to the $\Theta_{,ze}$ line with time during the night in Fig. 17b. The ridge-to-valley dimensions imply an advection timescale for CASES-97 ~5 times as long as that for AF for drainage winds of equal magnitude; the ratio becomes larger if their ''drainage'' scale of 3 km is used to represent the terrain. The relatively short delay time for the Mahrt et al. (2001) CASES-99 gully case could be a lower limit that reflects the timing of the onset of vertical mixing, which reduces the vertical temperature gradient as described in the foregoing. Indeed, data from the CASES-99 60-m tower show the strongest vertical temperature gradients in the first 3-h period after sunset (S. Burns 2002, personal communication). Because advection times differ according to the rate of cooling; the ambient wind direction; the slope of the terrain, the vegetative cover, and, at least in the present case, the asymmetry of the watershed and possibly independent flows within and above a cold pool at the base of the watershed, the relationship in Fig. 18 is true only in a general sense.

Second, if advection decreases horizontal variability, array size, station spacing, and local effects at the station sites would affect the time of maximum variability, because the horizontal variability would decrease first on small scales, and then on larger scales. The size of the measurement array defines the largest important terrain feature. If the array does not extend across the terrain feature, the observed advection time would be short-

Unauthenticated | Downloaded 08/01/21 08:40 PM UTC

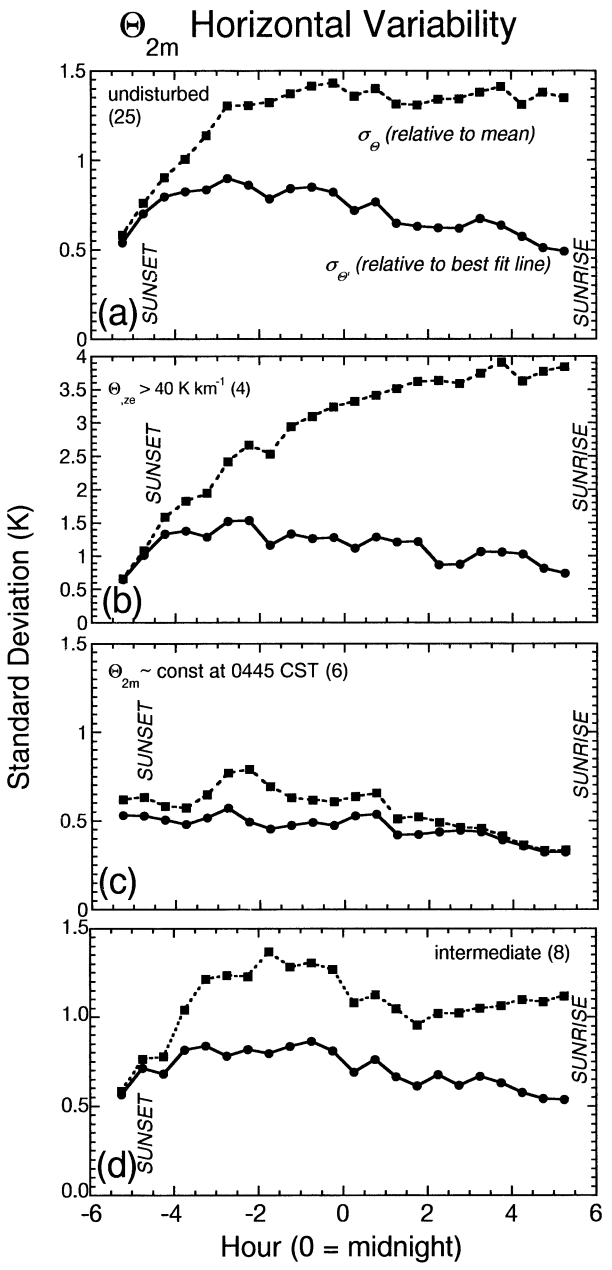

FIG. 17. For nights classified according to $\Theta_{,ze}$ during the half-hour period 0430–0500 CST, horizontal variability in Θ_{2m} as expressed by standard deviation σ_Θ relative to spatial mean (dotted line; squares), and standard deviation $\sigma_{\Theta'}$ relative to the $\Theta_{,ze}$ line (solid line; circles) for (a) all ''undisturbed'' nights (times with fronts, wind-shift lines or rain removed); and for (b) $\Theta_{,ze} > 40$ K km^{-1}, (c) $\Theta_{2m} \sim$ const($\Theta_{,ze} \approx 0$), and (d) $\Theta_{,ze}$ is intermediate. For (b), (c), and (d), nights with any disturbance were removed because of smaller sample sizes; (b)–(d) do not include nights with significant missing data.

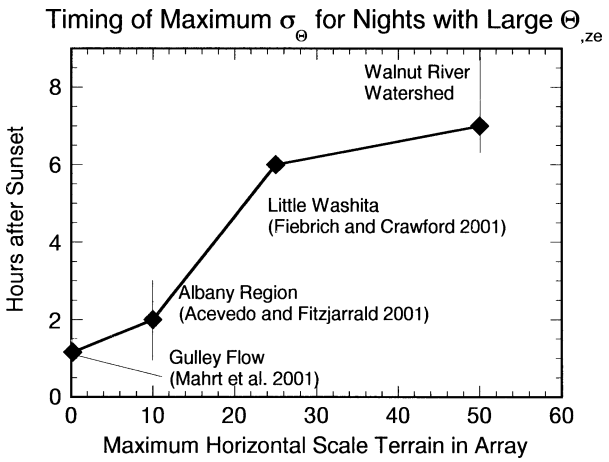

FIG. 18. Time between sunset and maximum horizontal variability σ_Θ as a function of the horizontal scale of the terrain, for nights with strong radiative cooling and light winds. For AF and the Walnut, the vertical lines represent the approximate range of values. Range for AF based on abstract and individual figures.

ened. The array spacing and siting strategy determine the amount of small-scale variability sampled. The array design in AF (spacing $\leq$ 5 km; AF, Fig. 3) captures more small-scale variability than CASES-97 (spacing 5–10 km; Fig. 1), but less than CASES-99 (inner spacing $<$100 m; Poulos et al. 2002). The undersampling of small-scale variability in CASES-97 is magnified by the siting of the flux stations in open areas to ensure adequate fetch for good eddy-correlation measurements, in contrast to the varied exposure of the AF stations due to nearby structures and trees as well as terrain features.

The effect of using half-hour average temperatures to evaluate horizontal variability, in contrast to the calculations of AF (1 min) and Fiebrich and Crawford (2001; 5 min), seems to be small for the stable cases. Comparing σ_Θ from 5-min and half-hour average values of Θ_{2m} for two of the cases, we find that both timing of the maxima and the magnitudes through the night are similar (not shown). This is consistent with the half-hour-averaged temporal standard deviations (based on the 10-Hz data) being much smaller (typically $<$0.5 K, with isolated values of $\sim$1 K), significantly less than the typical values of σ_Θ (3.5 K, from Figs. 17b and 5a).

The behavior is different for the constant-Θ_{2m} cases (Fr $\approx$ 3.3, from Fig. 11) illustrated in Fig. 17c: both spatial standard deviations are much smaller than for the large-$\Theta_{,ze}$ cases, with shallow peaks 2–3 h after sunset followed by a decrease until sunrise. The higher Froude numbers on these days result either from stronger winds or weaker radiative cooling compared to the very stable days. Either would accelerate the onset of the vertical mixing described by Businger (1973) or van de Wiel et al. (2002), reducing the impact of local radiative cooling, and allowing horizontal transport and vertical mixing to decrease horizontal variability. Also, advection time for these cases is less than half that for the stable cases (Fig. 8). The difference between σ_Θ and $\sigma_{\Theta'}$ indicates that, on average, $\Theta_{,ze} > 0$ until about 0230 CST.

The evolution of the Θ_{2m} standard deviations is strongly influenced by the changes of the wind through the night. Coincidentally, the onset of terrain-following

Unauthenticated | Downloaded 08/01/21 08:40 PM UTC

flow (0230 CST) is close to the time (0200 CST) that the southerly nocturnal low-level jet typically reaches a maximum (Whiteman et al. 1997). However, σ_Θ and $\sigma_{\Theta'}$ do not decrease monotonically. Examination of individual days shows that local maxima and minima reflect occasions when the surface layer flow at some of the stations is detached or recoupled to the ambient flow, as discussed by AF. As a rule, stronger winds were associated with less horizontal variability, regardless of time of night.

The standard deviations for the ''intermediate'' cases in Fig. 17d reflect a spectrum of examples between those dominated by drainage currents (reflected in the slight increase in horizontal variability after 0200 CST) and the constant-Θ_{2m} cases (reflected in a maximum in horizontal variability 3 h after sunset). Horizontal variability magnitudes are between those in Figs. 17b and 17c. Although average $\sigma_{\Theta'} \sim 0.5$ K in the predawn hours, the linear relationship between Θ_{2m} and elevation is weak on some nights. For example, Fig. 5 shows $\sigma_{\Theta'} \sim 1$ K on day 119 (29 April), only slightly less than σ_Θ(~1.5 K). As previously noted, a subsynoptic feature moving through the western part of the array probably affected the horizontal temperature distribution on this day. This does not imply that such features are associated with intermediate Froude numbers: the 14 May subsynoptic feature was followed by an early morning value of $\Theta_{,ze} \sim 0$ but with larger than typical $\sigma_{\Theta'}$. (This feature was sufficiently large horizontally to eliminate that night from the analysis.) On other nights, the temperature pattern could become disrupted as a subset of stations couples to the ambient flow when Ri becomes locally subcritical, as discussed in AF. While such seemingly random coupling events were evident during some nights, they do not have a significant effect in Fig. 5, where $\sigma_{\Theta'}$ is small for the remainder of the intermediate-$\Theta_{,ze}$ events.

Fiebrich and Crawford (2001) also found that horizontal variability of Θ_{2m} typically peaked just after sunset for both the Oklahoma mesonet, which spans hundreds of kilometers of surface terrain with elevation variation on scales up to ~50–100 km (Shaw and Doran 2001), and the Agricultural Research Service Micronet, which measures 20 km × 45 km. We suggest that the similarity of these results to those in Figs. 17c and 17d are related to the local climate: winds in Oklahoma are often strong, even at night.

6. The role of advection in the Θ_{2m} distribution

In this section, we provide a heuristic discussion of how Θ_{2m} that changes with time can remain constant horizontally for surface flow that is coupled to the ambient wind (coupled flow), and offer an explanation of the linear variation of temperature with elevation. If we follow an air parcel traveling over the surface, its potential temperature varies in response to vertical turbulence flux divergence and radiative cooling; that is,

$$\frac{d\Theta_{2m}}{dt} = -\frac{\partial \overline{w'\theta'}}{\partial z} - \frac{\partial R_{net}}{\partial z} \equiv F. \quad (3)$$

Assume that F varies little over scales large compared to trees and crops (3–5 km). This seems to be a reasonable assumption as long as the wind (and hence vertical mixing) varies little over the domain, because the terrain slope tends to be small (little geometric effect on radiative cooling) and land cover, over the eastern side of the watershed at least, is mostly grassland with some winter wheat and trees at the ends of fields or along creeks.

We first consider the case for which the ambient flow is coupled to the surface. From observations, Θ_{2m} is spatially constant under these conditions. Integrating (3) between t_0, the first time with coupled flow and constant Θ_{2m}, and an arbitrary time t_1,

$$\Theta_{2m}(t_1) - \Theta_{2m}(t_0) \approx \overline{F}(t_1 - t_0), \quad (4)$$

where $\overline{F}$ is averaged between t_0 and t_1. Under these conditions, air parcels traveling across the terrain with the ambient wind should cool (or warm) at the same rate at all locations. Since Θ_{2m} started out roughly constant, it should remain so, as observed. Thus, for coupled flow, Θ_{2m} can be constant in space without air parcels moving up and down with the terrain dry adiabatically. The *onset* of coupled flow and constant Θ_{2m} is a more complex issue that was qualitatively discussed earlier. In that case, air from higher up (more uniform because of its distance from the surface) mixing with near-surface air mutes horizontal variability, which is smoothed further as air parcels traveling over the terrain feel the effects of the representative types of surface over the watershed.

For drainage-flow conditions, we apply (3) to an air parcel traveling from the ridge top (location x_{ridge}, elevation z_{ridge}) to a position x_e at elevation z_e within a two-dimensional valley:

$$\Theta_{2m} = \int_{t_0}^{t_1} F\, dt = \int_{x_{ridge}}^{x_e} F \frac{dx_e}{U}, \quad (5)$$

where U is the speed of the downhill flow, which is approximately equal to the horizontal flow since the slope is small. Figure 8b suggests that U varies slowly for the elevations above the cold pool, and as noted in the foregoing, time variation is small on the nights considered. Under the assumption of a constant U,

$$\Theta_{2m}(x_e, t_1) = \Theta_{2m}(x_{ridge}, t_0) + \frac{\overline{F}}{U}(x_e - x_{ridge}), \quad (6)$$

where $\Theta_{2m}(x_{ridge}, t_0)$ is the potential temperature at ridge top at t_0. As seen from Figs. 2 and 5 of AF, $\Theta_{2m}(x_{ridge}, t)$ decreases approximately linearly with time;[5] that is,

[5] We assume a linear temperature decrease with time at the ridge top starting at t_0, the time at which the drainage current starts descending from the ridge. This time is probably shortly after the onset of cooling.

Unauthenticated | Downloaded 08/01/21 08:40 PM UTC

TABLE 2. Idealized Θ_{2m} (K) distribution on the side of a valley slope four units wide, with $F = -3$ K h^{-1} and $K = -1$ K h^{-1}, x-interval = 1 unit, and $U = 1$ unit h^{-1}. Shading indicates the area affected by air originating at the ridge top.

Time (hr)	$x = x_{ridge} = 0$ (ridge top)	$x = 1$	$x = 2$	$x = 3$	$x = 4$ (valley bottom)	$\Delta\Theta_{2m}$ (top-bottom)
0	300	300	300	300	300	0
1	299	297	297	297	297	2
2	298	296	294	294	294	4
3	297	295	293	291	291	6
4	296	294	292	290	288	8
5	295	293	291	289	287	8
6	294	292	290	288	286	8

$(\partial\Theta_{2m}/\partial t)(\underline{x}_{ridge}) = K$, where K is a constant. Note that $|K| < |\overline{F}|$ since the air feeding the drainage current at the ridge top must sink from higher up, where the cooling rate, primarily from radiative flux divergence, is slower. Using K = constant and replacing $t_1 - t_0$ with $(x_e - x_{ridge})/U$,

$$\Theta_{2m}(x_{ridge}, t_1) = \Theta_{2m}(x_{ridge}, t_0) + \frac{K}{U}(x_e - x_{ridge}). \quad (7)$$

Subtracting (6) from (7),

$$\Theta(x_{ridge}, t_1) - \Theta(x_e, t_1) = (K - \overline{F})\frac{x_e - x_{ridge}}{U}, \quad \text{or} \quad (8)$$

$$\Theta_{,ze} = \frac{K - \overline{F}}{U}\left[\frac{x_e - x_{ridge}}{z_{ridge} - z_e}\right]. \quad (9)$$

That is, Θ_{2m} increases linearly with elevation, as observed. We also see why advection time is important—(9) is satisfied only for parcels that started out at the ridge top.

It also follows from (8) that the time between sunset (or more strictly when the drainage current starts) and the time of maximum watershed-scale horizontal variability σ_Θ should increase with the scale of the watershed, as seen in Fig. 18. We present a simple example of this process in Table 2. In the table, it takes 4 h for the drainage-current air originating at the ridge top (shaded) to reach the valley bottom, cooling 3 K per space–time interval (one diagonal step in the table). Locations affected by air originating at the ridge top cool at 1 K h^{-1}, the same rate as at the ridge top. In areas not reached by this air, drainage-current air not originating at the ridge top also cools 3 K for each space–time interval; but results in a local cooling of 3 K h^{-1}, the same rate as at its point of origin (e.g., at $x = 1$ at hour 0, for the drainage-current parcel represented by the table cells just above the shaded cells). The horizontal variability increases until hour 4, at which time $\Theta_{,ze} = 8$ K/4 units, and then remains constant. We see similar behavior in Fig. 2 for 10 May, with the temperature falling more rapidly at the lowest than the highest station in the earlier hours of the night, but both cooling at the same rate in the last hours before sunrise.

However, the real situation is more complex. The idealized example is two-dimensional, and ignores the early evening increase in local variability and simply focuses on the large-scale variability associated with advective processes. Further, as noted previously, U, surface cover, terrain slope, and sampling strategies differ from case to case. When a cold pool is present, as in Fig. 9b, (9) strictly applies to the air parcel only until it encounters the cold-pool top.

7. Summary and conclusions

a. Horizontal variability in the last few hours before sunrise

We use data from eight NCAR surface flux stations to show that Θ_{2m}, the potential temperature Θ at 2 m AGL, varies linearly with elevation over the CASES-97 array during the hours just before sunrise. Based on data at 0330 and 0500 CST, $\Theta_{,ze} \sim \Theta_{,z}$ evaluated over 150 m, the elevation range of the surface stations and local terrain. There are several instances for which $\Theta_{,ze} \approx 0$ even though $\Theta_{,z} > 0$, consistent with surface layer air flowing up and down the terrain contours with the ambient wind (coupled flow) dry adiabatically in spite of positive static stability. In reality, the flow is coupled, but $\Theta_{,ze} = 0$ because Θ_{2m} changes everywhere in the watershed at the same rate. The natural logarithm of the Froude number is linearly related to $\Theta_{,ze}$; from this relationship, we find $\Theta_{,ze} \approx 0$ when Fr ≈ 3.3 (Fig. 11). This is surprisingly similar to the Fr ≈ 2 value that Mason (1987) and Holden et al. (2000) require for flow to be coupled to the terrain under stable conditions but in much steeper terrain (slopes 0.2—0.4, two orders of magnitude greater than for the Walnut River watershed) and based on slightly different methods of estimating Fr.

Froude numbers define the two broad flow regimes for the CASES-97 domain that are illustrated in Fig. 9. For Fr ~ 3.3, air flows up and down across the terrain contours and there is enough vertical mixing to couple the near-surface flow to the ambient wind and hence synoptic processes. For $Fr \ll 3.3$, the airflow is dominated by drainage flows up to watershed scale. Intermediate Fr values are associated behavior that is intermediate but not the average of the two extremes. The likelihood of vertical mixing events is higher than for the low-Fr (or high Ri) case, particularly at the higher stations, as seen in earlier studies by Acevedo and Fitzjarrald (2001).

Two factors lead to Θ_{2m} deviations from a linear change with elevation ($\Theta_{,ze}$ line): local surface characteristics (land cover and possibly terrain); and, for drainage-flow conditions, the development of a cold pool. Compared to values predicted by the $\Theta_{,ze}$ line, Θ_{2m} tends to be cooler over winter wheat and grass, and warmer

Unauthenticated | Downloaded 08/01/21 08:40 PM UTC

over bare ground. Over winter wheat, Θ_{2m} is up to ~0.5 K cooler because the zero-plane displacement height brings the temperature sensors ~0.6 m closer to the effective surface (G. Poulos 2000, personal communication). Also, the wheat insulates the soil and allows the air to cool, while the bare ground loses heat to the air (Oke 1987). The grasses insulate less than the taller, thicker winter wheat, and have smaller displacement heights. The association of downslope flows from nearby bluffs with cool departures at some sites does not necessarily imply causality, because the local flow is in the same direction as the watershed-scale drainage flow. Under very stable low-Fr conditions, systematic warm departures at stations 5 and 8 produce a kink in the z_e–Θ_{2m} profile that is probably related to the cold pool that develops at lower elevations. It is likely that cold pools form in some intermediate Fr cases as well.

b. Behavior through the night

Both the $\Theta_{,ze}$ lines and the relationships based on data through the night are less robust than those for the last hours before sunrise; $\Theta_{,ze} \sim 0.5\ \Theta_{,z}$ evaluated over 150 m, although the value of Fr required for flow coupled to the terrain remains about the same. The greater scatter during the earlier nighttime hours reflects the fact that the linear Θ_{2m} elevation pattern develops through the night. When all fair-weather cases are taken together, the spatial standard deviation of Θ_{2m} relative to the spatial mean (σ_Θ) increases for ~2 h after sunset, and then levels off, while the standard deviation relative to the $\Theta_{,ze}$ line ($\sigma_{\Theta'}$) reaches its smallest value just before sunrise. However, the evolution of horizontal variability in Θ_{2m} varies with early morning values of Fr.

- For low Fr, $\Theta_{,ze}$ increases on average through the night, while $\sigma_{\Theta'}$ reaches a maximum just after sunset and then decreases. Correspondingly, σ_Θ, on average, increases through the night—rapidly at first, and then more slowly, after ~6–8 hours—but maxima on individual days occur 6.5–9 h after sunset. Comparison of the CASES-97 data to similar studies indicates that the time required for σ_Θ to reach a maximum increases with the horizontal scale of the terrain in the instrument array.
- For Fr ~ 3.3($\Theta_{,ze} \approx 0$) by early morning, shallow maxima in both σ_Θ and $\sigma_{\Theta'}$ occur 2–3 h after sunset. We suspect the maximum variability is associated with the dominance of local processes at that time; reduction in horizontal variance later on results from the muting of local process by vertical mixing and advection, along with the tendency of the strongest winds of the night to occur in the early morning.
- For intermediate Fr, the standard deviations and time required to reach maximum horizontal variability represent a range of situations. As Fr increases, the influence of the ambient wind increases, implying a greater synoptic-scale influence. Examination of individual cases showed minimum horizontal variability associated with the strongest winds, reflecting mixing between near-surface and ambient air as suggested by AF.

Following an air parcel descending down the side of the valley and cooling by radiative and turbulence flux divergence, we show heuristically that a linear relationship between temperature and elevation develops for drainage flows, provided (a) total vertical flux divergence varies little on scales larger than a few kilometers, (b) the ridge top temperature cools linearly with time, and (c) drainage winds are nearly constant. If we add the assumption of (d) initial horizontally constant Θ_{2m}, the fact that the time between sunset and maximum spatial variability σ_Θ in a valley increases with the horizontal scale of the valley also follows from this argument, because the area of linear variation expands as the air from the ridge top progresses downhill. Applying similar reasoning to surface air parcels coupled to the ambient wind, we find that Θ_{2m} will remain constant under assumptions (a) and (d).

These results and those of other studies suggest the need for a synthesis of results from diverse sets of nighttime observations, and the design of new field experiments and numerical simulations to determine the limitations of our conclusions. The Froude or Richardson numbers are important in characterizing the behavior of the nocturnal surface layer, but Fr ~ 3.3 as a condition for surface layer flow up and down the terrain contours is almost certainly specific to the CASES-97 domain. Further, the variation with elevation in steeper mountainous terrain is not necessarily linear (D. Whiteman 2003, personal communication; Atkinson 1995). Several additional parameters must be considered, namely, the shape and scale of the domain and relevant terrain features, the height of the features (and hence slope), the location of the domain relative to those terrain features, the surface cover, and the local climate.

Acknowledgments. The authors wish to thank Marvin Wesely and Richard Coulter of Argonne National Laboratory, and Tom Horst and Tony Delany of NCAR for useful discussions, and Chin-Hoh Moeng, Greg Poulos, Joe Alfieri, and three anonymous reviewers for reviewing the paper and offering useful comments and useful background material. Finally, Larry Mahrt of Oregon State University and Ron Smith of Yale University provided helpful input. The comments from the three reviewers were useful and led to a better product. Kris Conrad helped prepare some of the figures. We also gratefully acknowledge NCAR ISFF for installing and maintaining the surface flux stations through CASES-97, and helping with the data afterward, and for collecting, correcting, and archiving the radiosonde data; and the Atmospheric Boundary Layer Experiments group at Argonne National Laboratory for installation and maintenance of wind profiling systems and archiv-

Unauthenticated | Downloaded 08/01/21 08:40 PM UTC

ing data afterward, and for answering our questions about the data. KI's support during this work was from the NCAR MMM CaSPP Program; RLG's support was from NSF-ATM Grant 9981811, and MWR's work was supported in part by the NCAR/MMM visitor's program.

REFERENCES

Acevedo, O. C., and D. R. Fitzjarrald, 2001: The early evening surface-layer transition: Temporal and spatial variability. *J. Atmos. Sci.,* **58,** 2650–2667.

Angevine, W. M., and J. I. MacPherson, 1995: Comparison of wind profiler and aircraft wind measurements at Chebogue Point, Nova Scotia. *J. Atmos. Oceanic Technol.,* **12,** 421–426.

——, P. W. Bakwin, and K. J. Davis, 1998: Wind profiler and RASS measurements compared with measurements from a 450-m tall tower. *J. Atmos. Oceanic Technol.,* **15,** 818–825.

Atkinson, B. W., 1995: Orographic and stability effects on valley-side drainage flows. *Bound.-Layer Meteor.,* **75,** 403–428.

Banta, R. M., and P. T. Gannon Sr., 1995: Influence of soil moisture on simulations of katabatic flow. *Theor. Appl. Climatol.,* **52,** 85–94.

Belcher, S. E., and N. Wood, 1996: Form and wave drag due to stably stratified turbulent flow over low ridges. *Quart. J. Roy. Meteor. Soc.,* **122,** 863–902.

——, and J. C. R. Hunt, 1998: Turbulent flow over hills and waves. *Annu. Rev. Fluid Mech.,* **30,** 507–538.

Blumen, W., R. L. Grossman, and M. Piper, 1999: Analysis of heat budget, dissipation, and frontogenesis in a shallow density current. *Bound.-Layer Meteor.,* **91,** 281–306.

Bossert, J. E., and G. S. Poulos, 1995: A numerical investigation of mechanisms affecting drainage flows in highly complex terrain. *Theor. Appl. Climatol.,* **52,** 119–134.

Businger, J. A., 1973: Turbulent transfer in the atmospheric surface layer. *Workshop on Micrometeorology,* D. H. Haugen, Ed., Amer. Meteor. Soc., 67–100.

——, J. C. Wyngaard, Y. Izumi, and E. F. Bradley, 1971: Flux profile relationships in the atmospheric surface layer. *J. Atmos. Sci.,* **28,** 181–189.

Campbell, G. S., and J. M. Norman, 2000: *An Introduction to Environmental Biophysics.* 2d ed. Springer-Verlag, 286 pp.

Carruthers, D. L., and J. C. R. Hunt, 1990: Fluid mechanics of airflow over hills: Turbulence, fluxes, and waves in the boundary layer. *Atmospheric Processes over Complex Terrain, Meteor. Monogr.,* No. 45, Amer. Meteor. Soc., 83–104.

Cornford, C. E., 1938: Katabatic winds and the prevention of frost damage. *Quart. J. Roy. Meteor. Soc.,* **64,** 553–591.

Coulter, R. L., and T. J. Martin, 1986: Results from a high-power, high-frequency sodar. *Atmos. Res.,* **20,** 257–270.

——, M. Orgill, and W. Porch, 1989: Tributary fluxes into Brush Creek Valley. *J. Appl. Meteor.,* **28,** 555–568.

Fiebrich, C. A., and K. C. Crawford, 2001: The impact of unique meteorological phenomena detected by the Oklahoma Mesonet and ARS Micronet on automated quality control. *Bull. Amer. Meteor. Soc.,* **82,** 2173–2187.

Fleagle, R. G., 1950: A theory of air drainage. *J. Meteor.,* **7,** 227–232.

Geiger, R., 1966: *The Climate Near the Ground.* rev. ed. Harvard University Press, 610 pp.

Gudicksen, T., J. M. Leone Jr., C. W. King, D. Ruffieux, and W. D. Neff, 1992: Measurements and modeling of the effects of ambient meteorology on nocturnal drainage flows—A numerical study. *Bound.-Layer Meteor.,* **38,** 315–337.

Harrison, A. A., 1971: A discussion of the temperatures of inland Kent with particular reference to night minima in the lowlands. *Meteor. Mag.,* **100,** 97–110.

Hocevar, A., and J. D. Martsolf, 1971: Temperature distribution under radiation frost conditions in a central Pennsylvania valley. *Agric. Meteor.,* **8,** 371–383.

Holden, J. J., S. H. Derbyshire, and S. E. Belcher, 2000: Tethered balloon observations of the nocturnal stable boundary layer in a valley. *Bound.-Layer Meteor.,* **97,** 1–24.

Jackson, P. S., and J. C. R. Hunt, 1975: Turbulent wind flow over a low hill. *Quart. J. Roy. Meteor. Soc.,* **101,** 929–955.

Laughlin, G. P., and J. D. Kalma, 1987: Frost hazard assessment from local weather and terrain data. *Agric. For. Meteor.,* **40,** 1–16.

——, and ——, 1990: Frost risk mapping for landscape planning: A methodology. *Theor. Appl. Climatol.,* **42,** 41–51.

LeMone, M. A., and R. L. Grossman, 2000: Mesoscale and diurnal variability of 2-m temperature and specific humidity in CASES-97. Preprints, *14th Symp. on Boundary Layer and Turbulence,* Aspen, CO, Amer. Meteor. Soc., 5–8.

——, and Coauthors, 2000: Land–atmosphere interaction research, early results, and opportunities in the Walnut River watershed in southeast Kansas: CASES and ABLE. *Bull. Amer. Meteor. Soc.,* **81,** 757–779.

——, and Coauthors, 2002: CASES-97: Late-morning warming and moistening of the convective boundary layer over the Walnut River watershed. *Bound.-Layer Meteor.,* **104,** 1–52.

Mahrt, L., and S. Larsen, 1982: Small scale drainage front. *Tellus,* **34,** 579–587.

—— and R. C. Heald, 1983: Nocturnal surface temperature distribution as remotely sensed from low-flying aircraft. *Agric. Meteor.,* **28,** 99–107.

——, J. Sun, W. Blumen, A. Delany, G. McClean, and S. Oncley, 1998: Nocturnal boundary-layer regimes. *Bound.-Layer Meteor.,* **88,** 255–278.

——, D. Vickers, R. Nakamura, M. R. Soler, J. Sun, S. Burns, and D. Lenschow, 2001: Shallow drainage flows. *Bound.-Layer Meteor.,* **101,** 243–260.

Martner, B. E., and Coauthors, 1993: An evaluation of wind profiler, RASS, and microwave radiometer performance. *Bull. Amer. Meteor. Soc.,* **74,** 599–613.

Mason, P. J., 1987: Diurnal variations in flow over a succession of ridges and valleys. *Quart. J. Roy. Meteor. Soc.,* **113,** 1117–1140.

Oke, T. R., 1987: *Boundary Layer Climates.* 2d ed. Methuen, 435 pp.

Poulos, G. S., and Coauthors, 2002: CASES-99: A comprehensive investigation of the stable nocturnal boundary layer. *Bull. Amer. Meteor. Soc.,* **83,** 555–581.

Shaw, W. J., and J. C. Doran, 2001: Observations of systematic boundary layer divergence patterns and their relationship to land use and topography. *J. Climate,* **14,** 1753–1764.

Smith, R. B., 1989: Hydrostatic airflow over mountains. *Advances in Geophysics,* Vol. 31, Academic Press, 1–41.

Sun, J., and Coauthors, 2002: Intermittent turbulence associated with a density current passage in the stable boundary layer. *Bound.-Layer Meteor.,* **105,** 199–219.

van de Wiel, B. J. H., R. J. Ronda, A. F. Moene, H. A. R. De Bruin, and A. A. M. Holtslag, 2002: Intermittent turbulence and oscillations in the stable boundary layer over land. Part I: A bulk model. *J. Atmos. Sci.,* **59,** 942–958.

Whiteman, C. D., X. Bian, and S. Zhong, 1997: Low-level jet climatology from enhanced rawinsonde observations at a site in the Southern Great Plains. *J. Appl. Meteor.,* **36,** 1363–1376.

Unauthenticated | Downloaded 08/01/21 08:40 PM UTC